https://doi.org/10.1016/j.mtener.2017.12.012

Zinc-based hybrid flow batteries: From fundamentals to applications

A.Khor, P. Leung, C. Flox, Q. Xu, L. An, A. Shah, R. Wills, M.R. Mohamed, J. Morante

Abstract

Zinc-based hybrid flow batteries are one of the most promising systems for medium- to large-scale energy storage application with particular advantages of cost, cell voltage and energy density. Several of these systems are the few flow battery chemistries being scaled-up and commercialized for different applications. The existing zinc-based systems relies on zinc electrodeposition in flowing electrolytes as the negative electrode reactions, which are coupled with organic or inorganic positive active species in either solid, liquid or gas phases. These reactions are facilitated with specific cell architectures under certain circumstances. To improve the performance and cycle life of these batteries, this review provides fundamental information of the zinc electrodeposition and summarizes the recent developments of the relevant flow battery chemistries and their recent applications. The future challenges and opportunities of this technology are discussed.

Keywords: Electrodeposition, hybrid flow batteries, redox flow batteries, zinc

1. Introduction

Redox flow batteries (RFBs) are an important contender for energy storage and load levelling for the electrical grid, especially in couple with sustainable energy sources, such as photovoltaic cells and wind turbines [1, 2]. Among various electrochemical technologies, this technology is considered as one of the most realistic candidate for energy storage in range of several kW/ kW h up to tens of MW / MW h. Conventional redox flow batteries, such as all-vanadium batteries, store energy in the form of reduced and oxidized electroactive species in the electrolytes, while at least one of the electrode reactions of the hybrid flow batteries involve a phase change in either solid or gaseous phases. Common examples are those systems based on metal electrodepositions and redox reactions of gaseous hydrogen and oxygen.

Despite the fact that the all-vanadium redox flow battery is the most developed system due to its high reversibility and relatively large power output, the electrolyte cost of such system is higher than USD$ 80 /kW h [3, 4]. The resulting capital cost can be up to USD$ 200 – 750 / kWh, which is far too high compared to the cost target (USD$ 150 /kW h by 2023) set by the United States Department of Energy (DoE) to match with existing physical energy storage technologies [5]. In order to reduce the costs of redox flow battery systems, recent investigations have highlighted the use of low-cost active materials sourced from both metallic and non-metallic (i.e. organic) compounds [6-8]. Compared to metallic materials, the development of the organic-based systems (redox flow batteries) are still relatively new (since 2009 [9]) and require tremendous improvements to address issues associated with low energy density (< 15 Wh dm^{-3}) restricted by both solubilities and cell voltages in the existing systems [6-8, 10].

On the other hand, low-cost metals (< USD$ 4 kg^{-1}) are still limited to the options of zinc, lead, iron, manganese, cadmium and chromium for redox/hybrid flow battery applications. Many of these metals are highly abundant in earth's crust (> 10 ppm [11]) and have annual productions of more than 4 million tons per annum (2016) [12]. The widespread availability and accessibility make these elements attractive for large-scale energy storage applications. With the exceptions of iron (Fe(II)/Fe(III)) and manganese (MnO_2/MnOOH) reactions, most of these metallic elements involve electrodeposition from dissolved species and mainly serve as negative electrode reactions. Among these elements, metallic zinc has the highest energy content due to its large volumetric

capacities (5.85 Ah cm^{-3}) and negative electrode potentials in aqueous media (acidic: –0.76 V *vs.* SHE; alkaline: –1.29 V *vs.* SHE) [13, 14]. In general, such negative electrode potentials imply side reaction of hydrogen evolution in the water electrolysis. However, zinc electrodeposition on inert substrates has been demonstrated as a relatively efficient process in aqueous electrolytes (both acidic and alkaline) with current efficiencies of over 90 % achieved attributed to its large hydrogen overportential and the suitable electrolyte compositions. This process is well established in the industry and has been used extensively in the areas of electroplating, corrosion protection and automotive vehicles [11, 12, 15-17]. At present, conventional baths for zinc electrodeposition are still mainly based on zincate (alkaline) [18], chloride (acid) [19-21] and sulfate [22-30] in the electroplating industry

In contrast, electrodepositions of other electronegative metals, particularly lithium, sodium and aluminum, are impossible in aqueous electrolytes and have to be carried out in non-aqueous solvents or room-temperature ionic-liquids. For large-scale energy storage, such as redox flow batteries, these solvents are less attractive in terms of cost and ionic conductivity (10^{-8} to 10^{-10} S cm^{-1} without salts). The low power density caused by poor ionic conductivity implies larger electrode size or more number of cells in a system required for a given power output, which leads to a significant increase in overall cost per kW h [31].

Furthermore, many of these solvents are flammable, rising concerns of safety while using with reactive metal anodes (i.e. lithium and sodium) at large scale. Together with its low-cost nature, zinc remains one of the commonest anode materials for primary and secondary batteries in consumer markets. Primary systems based on zinc anode were introduced near the beginning of battery technology – Leclanché wet cells (zinc-manganese dioxide) in 1866 [13]. Since the past decades, zinc-carbon and zinc-alkaline dry cells (zinc-manganese dioxide) are still used in various portable devices [14].These batteries are often associated with one-time use as primary cells, although rechargeable systems are available. The poor reversibility was attributed to the cycling-induced changes of materials in both anode and cathode (manganese dioxide) materials [32, 33]. In conventional static systems, dendritic morphologies of zinc anodes tend to develop at limiting current densities caused by the non-uniform concentration gradients [34]. Therefore, controlling mass transport by convection as used in a flow battery configuration has been demonstrated as an effective approach to improve the morphology and extend the cycle life by minimizing dendritic growth, shape change and passivation of zinc electrodes [34, 35].

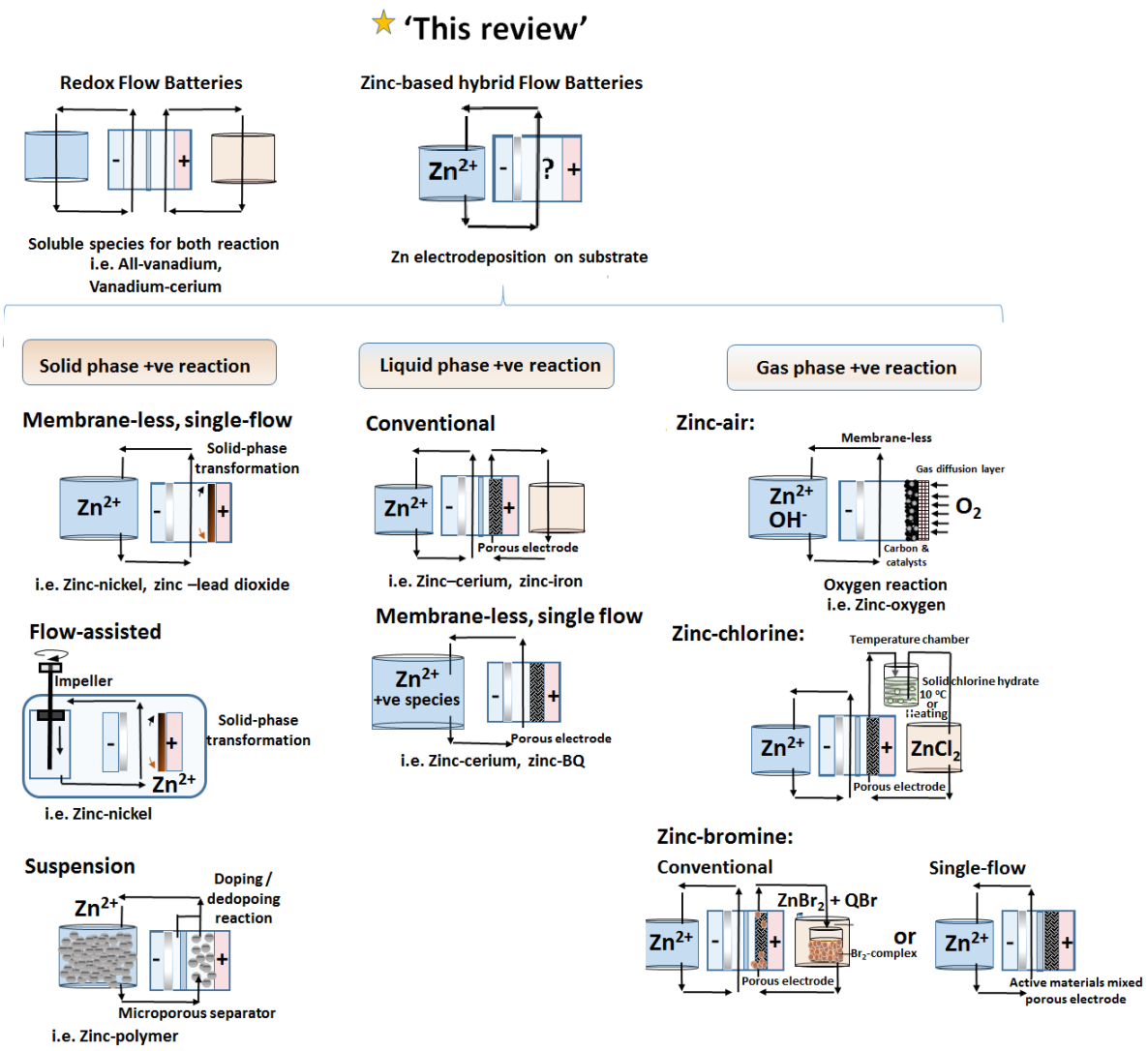

Figure 1 (a) Zinc system with solid phase reaction, (b) liquid state reaction, (c) and gas phase reaction

Since the 1970s, various zinc-based flow batteries have been proposed and developed by coupling with different positive electrode reactions [36]. Together with all-vanadium, zinc-based systems are the few flow battery chemistries being scaled-up and commercialized for different applications. The existing zinc-based systems use positive electrode reactions based on inorganic or organic active materials in either solid, liquid or gas phases. These reactions are facilitated with specific cell architectures under different circumstances. In all systems, the negative electrode reaction relies on zinc electrodeposition, which takes place in flowing electrolytes as in other hybrid flow batteries. This highlights the importance of the zinc electrodeposition process and the necessity of obtaining suitable deposit morphologies for long-term cyclings.

In many of these systems, separators or membranes are used to prevent direct reaction or crossover of the charged species between the two half-cell compartments. However, the involvement of at least one solid-phase electrode reaction (including zinc electrodeposition) in zinc-based systems provides a possibility of 'membrane-less' configuration. In certain chemistries, the positive electrode reactions do not involve soluble species and undergo pure solid-phase transformation, while some others make use of slow dissolution of zinc electrodeposit in the presence of certain active species dissolved in the electrolytes, particularly at low concentrations.

However, most of these zinc-based systems still face challenges of self-discharge, electrode shape-change and formation of dendrites. All these need to be further minimized for improved performance and cycle life. In order

to advance the existing technologies, it is essential to improve the understanding of the zinc electrodeposition process and gain knowledge from previous experiences. At present, there are a number of review articles have been published in the field of redox flow batteries, regarding general chemistries [1, 2, 31, 37-41], cell architectures [42], mathematical modellings [43] and cost analysis [4, 44]. Specific systems based on attractive elements, such as vanadium [45-47], lithium [48] and organic materials [6, 7], have been recently reviewed. In contrast to previous reviews, the present contribution provides an overview of the zinc electrodeposition process and a comprehensive summary of the existing zinc-based flow battery technologies and their recent applications. The latest advances, future challenges and opportunities for further development are discussed.

2. Electrochemistry of zinc electrodeposition

Zinc is a moderately reactive bluish-grey metal, can be found in nature as sphalerite, smithsonite, hemimorphite and franklite ores [49]. The atomic number and weight of this element are 30 and 65.38 respectively. Pure zinc is neither particularly ductile nor malleable. Its density is 7.14 g cm^{-3} with electrical resistivity of 6.16 μΩ cm^{-1} and melting point of 419.5 °C [50]. The electrode potential is associated with the operating parameters and the activities of the reactants governed by the Nernst equation. In general the standard electrode potentials of zinc are –0.76 V and –1.29 V in acidic and alkaline media, respectively. Given the dependence of chemical activities on other thermodynamic parameters, the equilibrium electrode potential separate the oxidized/ reduced phases on a phase diagram. As shown in Figure 2, Pourbaix diagram as a certain class of phase diagrams is displayed by the equilibrium potential plotted against the pH, when some of the reactants have chemical activities that vary with pH in aqueous electrolytes. This is useful to determine which species is thermodynamically stable at given potentials and pHs but does not provide information about the kinetics of the reaction processes.

Pourbaix diagrams for zinc have been published by a number of authors and vary with temperatures and electrolyte compositions [51-53]. For most existing zinc-based hybrid flow batteries, charge or electrical energy is mainly stored as an electrodeposit in the reduction process. As shown in Figure 2, metallic zinc is electrodeposited in four different routes through reactants as forms of Zn^{2+}, $Zn(OH)_2$, $HZnO_2^-$ and ZnO_2^{2-}. Depending on the pHs of the aqueous electrolytes, the formations of $Zn(OH)_2$, $HZnO_2^-$ and ZnO_2^{2-} are often caused by the hydrolysis of Zn^{2+}. It is important to note that the traditional notations of $HZnO_2^-$ and ZnO_2^{2} in most Pourbaix diagrams correspond to the hydrolysed zinc complexes of $Zn(OH)_3^-$ and $Zn(OH)_4^{2-}$ used in most battery equations.

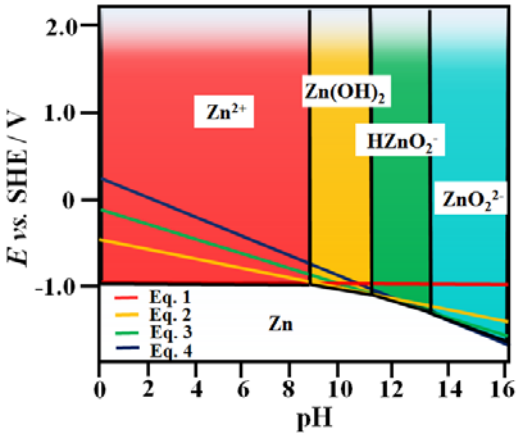

Figure 2 Pourbaix diagram for zinc in different pH in water.

Nernst equation can be written for each of these reactants in equilibrium with metallic zinc.
In the media of water at different pHs:

$$Zn^{2+} + 2e^- \leftrightarrow Zn$$
$$E_e = -0.763\ V + 0.0295\ V \log [Zn^{2+}] \quad (1)$$

$$Zn(OH)_2 + 2H^+ + 2e^- \leftrightarrow Zn + 2H_2O \quad (2)$$

$$E_e = -0.439\ \text{V} - 0.0591\ \text{V pH}$$

$$HZnO^{2-} + 3H^+ + 2e^- \leftrightarrow Zn + 2H_2O$$
$$\text{E}_e = 0.54\ \text{V} - 0.0886\ \text{V pH} + 0.0295\ \text{V log}\ [\text{HZnO}^{2-}] \quad (3)$$

$$ZnO_2{}^{2-} + 4\,H^+ + 2e^- \leftrightarrow Zn + 2H_2O$$
$$\text{E}_e = 0.441\ \text{V} - 0.1182\ \text{V pH} + 0.0295\ \text{V log}\ [\text{ZnO}_2{}^{2-}] \quad (4)$$

The Nernst equation for reaction (1) shows that it is independent of pH, which corresponds to a horizontal line at –0.763 V *vs.* SHE in the Pourbaix diagram. In contrast, the other electrodeposition routes (reactions (2-4)) vary linearly with pH at negative gradients. Based on these equations, the Pourbaix diagram can be divided into four regions, corresponding to different reactants being thermodynamically stable in the electrodeposition processes. These vertical lines between these four regions are independent of electrode potential and can be calculated by considering the equilibrium constant [52]:

pH ≈ 8.5

$$Zn^{2+} + 2H_2O \leftrightarrow Zn(OH)_2 + 2H^+ \quad (5)$$

pH ≈ 10.7

$$Zn(OH)_2 \leftrightarrow HZnO_2{}^- + H^+ \quad (6)$$

pH ≈ 13.1

$$HZnO_2{}^- \leftrightarrow ZnO_2{}^{2-} + H^+ \quad (7)$$

In the presences of different anions or salts (i.e. chloride, bromide), the formations of these complexes could take place at slightly different pHs. For instance, in the presence of chloride, the Pourbaix diagram is still very similar to that in pure water. However, in the presence of bromide salts, the region of Zn^{2+} species ($ZnBr_3^-$) stability is *c.a.* pH 6 (*vs. c.a.* pH 8.5 in equation (5))

Hydrogen reactions (evolution or oxidation) could compete or pair with zinc electrodeposition/ dissolution processes to make a local net reaction. When zinc or other metals (particularly those of the current collectors) exposed to the electrolytes containing protons/ acid, dissolution of these metals take place as a form of corrosion with hydrogen evolutions at open-circuit due to the following mixed electrode reactions on the metallic surface [54]:

$$M - ne^- \leftrightarrow M^{n+} \quad (8)$$

$$2H^+ + 2e^- \leftrightarrow H_2 \quad (9)$$

Similar to the case of proton, metallic zinc also reacts with the active species oxidized by the positive electrodes, resulting in energy loss. For this reason, separators are used to prevent the crossover of the active species between the two half-cells. For a few cases [55-57], no membrane is actually needed when these positive electrode reaction do not involve soluble species and undergo solid-phase transformation ($NiOOH/Ni(OH)_2$ [55, 56], $PbO_2/PbSO_4$ [57]). Furthermore, metallic zinc can be protected by mean of cathodic protection in the electrodeposition process. Therefore, the dissolution of zinc takes place only at open-circuit or in the discharge process. Based on this concept, membrane-less systems [58-61] could be possible and have been introduced recently by making use of slow dissolution of zinc in the presence of particular active species at low concentration (< 0.5 M).

However, corrosion or dissolution of metallic components of redox flow battery is detrimental for long-term operation and performance. The dissolved metal ions could lead to unstable redox potentials and distort the

original chemistries of the flow batteries. Together with the weight issues, metallic components are not commonly used in most flow battery systems. In comparison, carbon and polymer based materials are used as electrodes and cell components, respectively, as these materials do not undergo dissolution or formation of oxides in the oxidation process [62, 63]. Although carbon-based materials can be eroded in the oxidation reactions by mean of carbon dioxide evolutions [64], these materials are suitable for most negative electrode reactions even under excessive hydrogen evolutions [65]. In contrast to the electroplating industry, where majority of substrates are metals, carbon-based substrates are extensively used in hybrid flow batteries. Since pure carbon/graphite is brittle and often difficult to scale up in stacks, composites of polymer binders and conductive particles [66-69] are often used instead [66-69].

In typical linear sweep voltammetry, zinc electrodeposition can take place in three regions at a condition that electrolyte flow is static and hydrogen evolution is not particularly dominant (Figure 3). In region I, the initial deposition rate is usually slow and attributed to charge transfer control. While in region II, the current density increases then decreases dramatically at more negative electrode potential, resulting in a cathodic peak due to diffusion control. After this, a sharp increase in current density is obtained in region III associated with hydrogen evolution together with the electrodeposition process. In such region, zinc electrodeposition is dominantly under mass transport control rather than charge transfer control. When the electrode potential sweeps towards even more negative values, hydrogen evolution becomes dominant and appears as a significant side reaction [70].

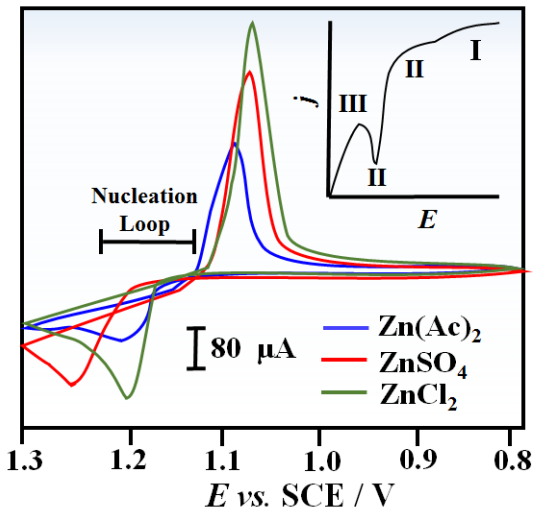

Figure 3 Linear sweep voltammetry for Zn $(Ac)_2$, $ZnSO_4$ and $ZnCl_2$ [70, 71].

However, these cathodic potentials could vary with different electrolyte compositions, particularly anion and pH. Figure 3 shows the cyclic voltammetry of zinc electrodeposition on glassy carbon electrode from solutions of different anions (acetate, chloride and sulphate) in neutral solutions [71]. In each curve, the forward and reverse scans form a nucleation loop between the cathodic and anodic peaks, which has been ascribed to the nucleation process requiring an activation energy provided by an overpotential [72]. Among these curves, it can be seen that the cathodic peak potential of zinc chloride solution is similar to that with acetate anions, while the peak current of chloride solution is the largest among the three solutions. This shows that the effect of chloride ions (Cl^-) on the zinc electrodeposition overpotentials is similar to that of acetate ions on that glassy carbon substrate. In contrast, the cathodic peak potential of the sulphate solution is the most negative, which is about 50 mV more negative from those peaks in the other two solutions. This suggests more difficult electrodeposition process in sulphate solutions. Such an overpotential can be explained by the strong interaction between sulphate and zinc (II) ions as reflected by its positive stability constant ($\lg \beta = 2.3$). The overpotential is considered as the driving force of electrocrystallization at the electrode surface, which include adsorption, nucleation and growth processes

[24], which is also sensitive to the zinc(II) concentration [19] as well as the identity of additives [27-30]. The mechanisms of these phenomena have been discussed in details by previous researchers [73-81].

In general, the competition between growth and nucleation determines the granularity of the electrodeposit. The higher the nucleation rate caused by the overpotential during the electrodeposition process, the finer the crystal grains of the deposit. On the other hand, the forms of growing crystals at the growth centres determine the general appearance and structure of the electrodeposits as illustrated in Figure 4**.** Since the over-potential is the derivation of the electrode potential from its equilibrium value, poor control of potential distribution often result in undesirable morphologies (i.e. dendrites) and growth rate.

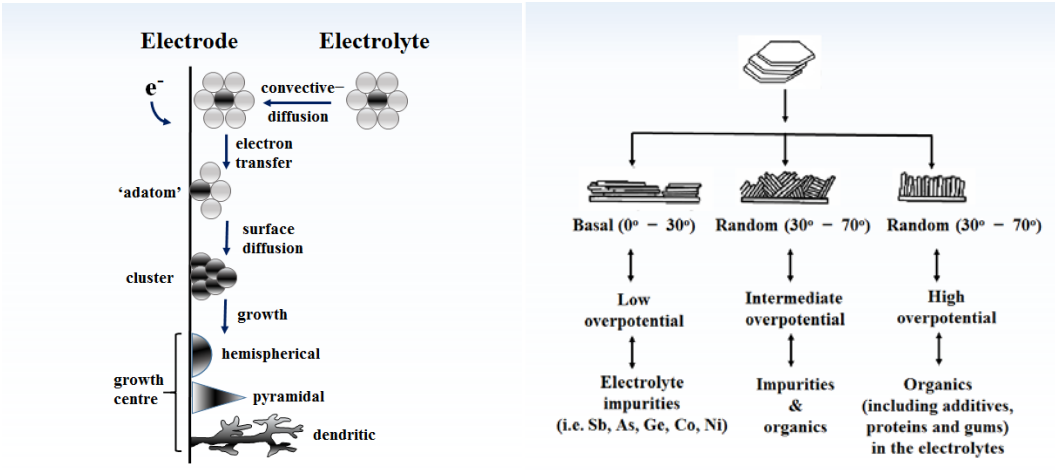

(a) (b)

Figure 4. (a) The growth mechanisms of zinc electrodeposition; (b) the relationships among overpotentials, impurtities and electrolyte additives and the crystallographic growth of the zinc electrodeposits.

The relationships among overpotentials, impurities, and electrolyte additives (organic), and the crystallographic growth of the electrodeposits are shown schematically in Figure 4 [74, 82]. This is consistent with the study of Raeissi *et al.* [83] that increasing overpotential results in a decrease of basal plane and increase of low angle planes in zinc sulphate electrolytes (pH 2). Zinc electrodeposits are generally classified into 5 categories: heavy spongy, dendritic, boulder, layer-like, and filamentous mossy [84].

Based on the electrodeposit crystallinity and microstructure, these 5 categories are summarized in Table 1, while the microscopic images of these distinct morphologies are shown in Figure 5 (electrodeposits obtained from alkaline electrolytes). Based on the examples of zincate solutions, heavy spongy morhologies are large boulder agglomerates and highly branched dendrites, developing at high current densities and after prolonged deposition. Dendritic structures are treelike and sometimes hexagonal if the rate of electrodeposition is slow, while boulders are typically hexagonal shape in discrete assemblies. Layerlike structures are formed by epitaxial growth in the early stage of the deposition process, while hexagonal platelets have been reported extensively in acidic solutions [29, 85, 86]. Filamentous mossy deposits have the appearance of tangled whiskers with a typical diameter of 50–200 nm and lengths that may exceed 5 μm.

In zinc bromide solutions, mossy morphologies are often observed in weakly acidic and basic conditions [87, 88], which are considered undesirable for battery operations. To address the morphological issues, organic and inorganic additives are commonly used in both areas of electroplating and battery applications. In general, organic additives increase the electrode overpotentials by their adsorption or partial covering at the electrode surfaces [28-30, 35, 85, 86], which block the growth of the zinc crystals. On the contrary, some inorganic additives, such as indium oxide, may exhibit high hydrogen overpotential [54, 89]. Despite the improved or more uniform morphologies, zinc electrodeposition may also be inhibited by some organic additives (i.e. surfactants), resulting in low half-cell coulombic efficiencies [35, 86]. However, some electrodeposits are found to contain high content

of carbon due to the presence of organic additives and the possible impurities in the electrodeposition processes [82, 90].

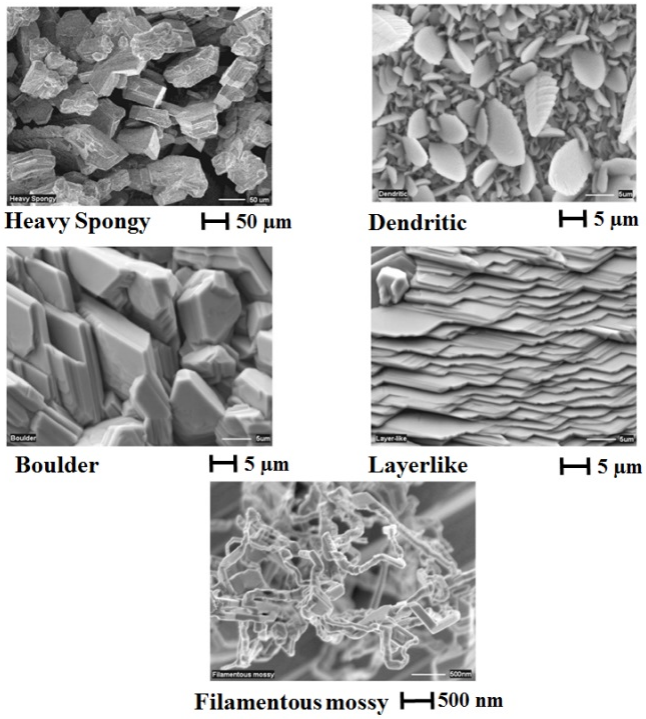

Figure 5 illustrates different types of zinc deposition (heavy spongy, dendrite, boulder, layerlike and filaentous mossy) on electrode surface (electrodeposited through alkaline electrolytes) [84].

Category of zinc deposit morphology					
Property	**Heavy spongy**	**Dendritic**	**Boulder**	**Layer-like**	**Mossy**
Appearance	Black powder	Metallic crystal	Grey metal	Reflective metal	Black powder
Microstructure (under microscope)	Agglomerate large boulder	Fern, leaf, hexagon	Granular boulder	Ridge, layer like	Filament, whisker
Adherence	Non-adherent	Non-adherent	Adherent	Adherent	Non-adherent
Porosity	Dispersed	Dispersed	Compact non-porous	Compact non-porous	Highly porous
Crystallinity*	Anisotropically oriented	Isotropically oriented	Anisotropically oriented	Epitaxial oriented	Isotropically oriented
Growth current density	Highest	Very high	Moderate	Low	Lowest

Nucleation site selectivity	Non-selective	Non-selective	Selective	Non-selective	Highly selective

*Anisotropically oriented: deposits grow three-dimensionally; bulk and individual deposits are polycrystalline. Isotopically oriented; deposits grow two-dimensionally; individual deposits are single crystals.

Table 1 Categories of zinc deposit morphology[84].

3. Improving zinc electrodeposit morphologies for hybrid flow batteries

Improved zinc electrodeposit morphologies are essential for long-term charge-discharge cycling at reasonable performances. Dendritic growth is an undesirable feature of zinc electrodeposition, which entails the risk of damage to the separator and potential electrical short-circuit and self-discharge. Dendritic growth is usually developed from mossy to pyridimal/ acicular form. The overall growth and propagation of dendrites are influenced by the diffusion and the type of the zinc complexes [91, 92]. There are usually two main source of convective diffusions: (1) density differences between zinc ions and other compositions, and (2) local forced convection driven by hydrogen evolutions. These local convections lead to enhance the rate of dendrite propagation, while formation of dendrite is suppressed with the addition of electrolyte additives.

In zinc electroplating industry, electrolyte additives are used to obtain finer grain size, hence brighter the electrodeposit [93]. These additives tend to promote the 2-dimensional growth of crystallites [94]. Previous theories suggest that higher deposition overpotential could lead to faster nucleation rate and finer crystal grain sizes [95]. Electrolyte additives, particularly those with larger organic molecules, are often used to increase the deposition overpotential by partly covering and selectively absorbing on the electrode surface, which tend to prevent further grain growth and promote nucleation [96]. This also depends on the structure and the size of the additives, additive-substrate interactions and those between the additive and the deposit [97].

These electrolyte additives also influence the activation energy [98] and the rate of charge transfer [99]. The relationship between the current density and the electrolyte additive concentration has been established [100-102], which further influences the nucleation and crystallization of the electrodeposits [102]. In electroplating industries, some additives are regarded as ‘brighteners’, such as those called primary and carrier brighteners, which usually have large molecules and have rapid adsorption-desorption property [103]. Some are known as “levellers”, which are usually with smaller molecules and have specific adsorption at the electrode surface [104].

As developed by early theories [105], diffusion of these ‘levellers’ for entering the ‘peaks’ is faster than that of entering the ‘valleys’ in the microprofile of zinc electrodeposits. This results in higher ‘leveller’ concentrations at the ‘peaks’, where inhibition of electrodeposition occurs. On the other hand, metallic atoms migrate and electrodeposit on the recessed areas, therefore true levelling can be achieved [106]. However, suitable concentration of these ‘levellers’ is essential to achieve such effect [105, 107, 108].

4. Types of zinc-based hybrid flow batteries

4.1. Positive redox couples involving solid phase active materials

Solid-phase active materials, such as lead-dioxide and nickel hydroxide, do not involve soluble active species in the electrolytes and undergo pure solid-phase transformation from one solid to another in the charge-discharge processes. Since the charged products, including zinc electrodeposit, are at the electrode surface, separator and membrane are not needed to prevent direct reaction between these charged products. The resulting electrolytes only contain soluble zinc(II) species and serve as common electrolytes for both half-cell reactions. Compared to conventional static systems based on zinc oxide electrodes, flowing electrolyte are still necessary to extend the cycle life to more than several hundred cycles by addressing issues associated with dendrites, shape change and passivation at the zinc electrodes [109], resulting in flow-assisted [110] or single flow [55] architectures under

different circumstances. The capacities of these systems are still limited by the amount of the zinc electrodeposit at the negative electrode and the amount of solid active materials used in the positive electrode reactions.

4.1.1. Zinc-nickel

The concept of alkaline zinc-nickel rechargeable batteries can be traced back to the 1900s [111]. The development of the original static system has been associated with the relatively long cycle life of cadmium-nickel batteries (or nickel-cadmium batteries). In comparison, the zinc-nickel static battery has a higher cell voltage and exhibit a moderate specific energy of 55 – 85 Wh kg^{-1} [112] for high power applications (i.e. bicycles, scooters and electric vehicles). In conventional static systems, the nickel (hydroxide) electrode is usually sintered or pressed, while zinc electrode is made of finely porous matrix of zinc oxide at discharged state with the use of pressing method. In most cases, polymer or cellulose based separators are used to prevent the short circuit caused by dendritic growth.

The overall electrode reactions can be described as follows:
At positive electrode:

$$2NiOOH + 2H_2O + 2e^- \leftrightarrow 2Ni(OH)_2 + 2OH^- \text{ , } E^0 = 0.49 \text{ V } \textit{vs.} \text{ SHE} \quad (10)$$

Overall reaction:

$$Zn + 2H_2O + 2NiOOH \leftrightarrow 2Ni(OH)_2 + Zn(OH)_2 \text{ , } E_{cell} = 1.73 \text{ V} \quad (11)$$

In the presence of separators, the capacities of most static cells using zinc oxide electrodes (rather than zinc electrodeposition) often deteriorate over several hundred cycles primarily due to the internal short circuit [109, 110, 113, 114]. The use of flowing electrolyte is considered as an effective approach to address these issues associated with dendrite, shape change and passivation at the zinc electrode. In a flowing system, a separator is not necessary when an inter-electrode gap of > 4 mm is used [110, 113, 114], which reduce the overall cost and simplifies the cell design.

Early investigations include a 100 A h battery developed by Bronoel *et al.* [114] with the functions of pulsed charging and inversion of electrolyte directions. In 2007, a 'hybrid flow battery' concept has been introduced by Cheng and co-workers [55, 115] through fundamental studies [55] and lab-scale testings, in which more than 220 cycles have been obtained with the energy efficiencies of *c.a.* 88 %. In these works, cadmium was used as the substrate materials for zinc electrodeposition due to its relatively large hydrogen overpotential.

Following these, Ito *et al.* [110, 113] further evaluated the performance of a flow system with particular focus on the morphology evolutions during charge-discharge cycles. Due to the fact that zinc electrode reaction has higher coulombic efficiency than its nickel oxide counterpart, residual zinc tend to accumulate on the substrate or deposit surface after each cycle. Depleted zincate ions in the electrolytes and continuous hydrogen evolutions at the electrodeposit surface further facilitate the dendritic growth, which is often initiated at the regions of high local current densities at the microprofiles. In subsequent cycles, dendritic growth tends to take place progressively and may not be suppressed by the flowing electrolyte (Figure 6). However, dendritic growth may not cause serious internal shorting as long as there is no strong contact with the positive electrodes. These dendrites might peel off from the electrodeposit under aggressive flows. To avoid these, reconditioning of battery was introduced by conducting a deep discharge to fully remove or dissolve all the accumulated zinc electrodeposit every 15 cycles. Through these procedures, 1500 charge-discharge cycles have been obtained with energy efficiencies of over 80 %.

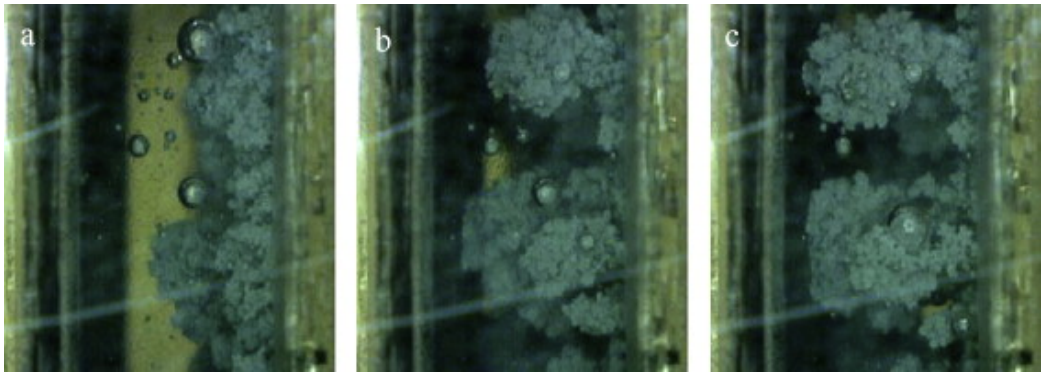

Figure 6. Electrodeposition of zinc on a planar carbon substrate under flowing electrolyte (V = 2 cm s^{-1}): (a) 1st cycle; (b) 5th cycle; (c) 9th cycle.

In addition to planar electrodes, several researchers [116-118] have proposed the uses of three-dimensional nickel foam as the negative electrodes to increase the current densities and cycle lives. Cheng *et al.* [116] demonstrated that it is possible to enable reasonable energy efficiencies (i.e. > 50 %) at ultra-high current densities of up to 300 mA cm^{-2}. Within these porous structures, the morphologies undergo from smooth (Fig. 7a), spongy (Fig. 7b–e) to dendrite structures (Fig. 7f) by increasing the current densities from 40 to 300 mA cm^{-2}. Although no further cycling information is provided, the other work of these researchers [117] concluded that extended cycle life was achieved with no accumulation of zinc observed within the porous structures for more than 400 cycles.

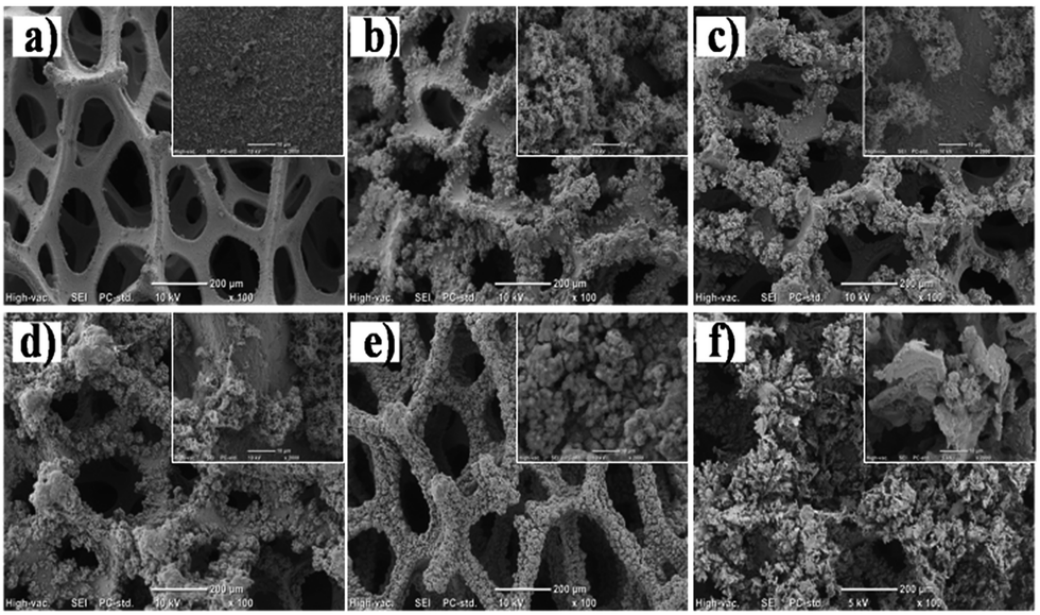

Figure 7. Zinc electrodeposit morphologies within porous nickel form structures at different current densities: (a) 40 mA cm^{-2}, (b) 80 mA cm^{-2}, (c) 120 mA cm^{-2}, (d) 160 mA cm^{-2}, (e) 200 mA cm^{-2}, (f) 300 mA cm^{-2}.

Based on the established laboratory-scale batteries, a scaled-up prototype has been developed by Turney *et al.* [119]. That system was up to 25 kW h consisting of thirty 833 W h batteries in series connections. The overall voltage ranged from 40 to 60 V with energy efficiency of more than 80 % over 1000 cycles, which is approximately a year of data (three cycles per day). In that system, the energy used for electrolyte pumping was only *c.a.* 4 % of the total energy throughput [119].

Despite tremendous improvements of recent studies, the discharge duration and capacities of these systems were typically limited to less than 4 h and 50 mA h g^{-1}, respectively. These were mainly attributed to the limited capacity of the nickel positive electrodes (< 50 mA h g^{-1}), while negative electrode reactions have been demonstrated under prolonged charge in other alkaline systems (240 – 500 mA h cm^{-2}) [120, 121]. Therefore, these features are not competitive with the conventional flow battery systems that store energy partly or fully through the electrolytes. This kind of batteries has been described as 'flow-assisted' battery rather than 'flow battery, in which the cell architecture are also different (See [110, 113, 119]). Instead of using filter-press type cells with specific manifolds to distribute electrolytes and to avoid shunt (bypass or leakage) current in a stack, electrode plates were immersed in the electrolyte, which was circulated within a sealed system [110, 113, 119]. Battery performance can be further improved with the uses of additives [122, 123], electrolytes [124, 125], electrodes [116-118] and battery architectures [126] as reported in existing studies of static and flow systems. Due to the use of positive nickel electrodes, the cost of this system is still more than USD$400 / kW h, significantly higher than the DoE cost target (USD$ 150 / kW h).

4.1.2. Zinc-lead-dioxide

The concept of acidic zinc-lead dioxide battery can be traced back to the 1970s in the description of a few patents [127-129]. This chemistry is based on low-cost elements in aqueous electrolytes and exhibit high open-circuit voltage (*c.a.* 2.45 V), which offers one of the highest cell voltages in aqueous electrolytes (20 % higher than conventional lead-acid batteries).

The overall electrode reactions can be described as follows:
At positive electrode:

$$PbO_2 + 2H^+ + H_2SO_4 + 2e^- \leftrightarrow PbSO_4 + 2H_2O \; E^0 = +1.36\text{V } \textit{vs.}\text{ SHE} \quad (12)$$

Overall reaction:

$$PbO_2 + Zn + 2H^+ + H_2SO_4 \leftrightarrow PbSO_4 + Zn^{2+} + 2H_2O \quad E_{cell} = 2.12\text{ V} \quad (13)$$

In contrast to most lead-dioxide based batteries, most aqueous systems are limited to less than 1.5 V due to the gaseous evolutions in the water electrolysis process. Together with lead-acid batteries (*c.a.* 2.05 V), the relatively high cell are contributed by the highly positive electrode potential of lead-dioxide reaction (+1.69 V *vs.* SHE). Considering voltages that lead(II) ion is almost insoluble in sulfuric acid (< 6.5 mg L^{-1}), any electrodeposition associated with lead(II) ions is negligible [57]. Therefore, zinc or other metals can be electrodeposited from soluble species in common electrolytes, serving as the negative electrode reactions of several proposed static or flow batteries (zinc-lead-dioxide [57, 130, 131]; copper-lead-dioxide [132]; cadmium-lead-dioxide [133]). Since the charged products are on the electrode surfaces, no membrane or separator is necessarily required to prevent direct chemical reactions of these products.

In the past decades, the zinc-lead dioxide chemistry has not received much attention due to zinc corrosion and the limited current densities (< 10 mA cm^{-2}) reported in the early systems [130]. In a recent static system, experimental results show that the average coulombic and energy efficiencies were up to 90 % and 70 %, respectively, over 90 cycles at 20 mA cm^{-2} [57]. Since thin carbon polymer electrode (0.6 mm thickness) were used instead of heavy metallic electrode materials, the specific energy was about 30 % higher than that of a commercial lead-acid batteries at the same operating conditions [130]. Following these, Pan *et al.* [131] has developed a membrane-less flow batteries based on single flow configuration. It was found that hydrogen evolution can be effectively suppressed with the doping of a polymer resin within the graphite composite. However, in charging process, protons are continuously generated as described in equation 12, which implies challenges in zinc electrodeposition and corrosion at the negative electrode. The proposed system also suffer from the limited capacities of lead-dioxide electrodes (< 50 mA h cm^{-2} [57]). To compete with other flow battery

chemistries, further developments of high-capacity positive electrodes and corrosion inhibitors are necessary for practical applications.

4.1.3. Zinc-polymer (suspensions)

The concept of zinc-polymer rechargeable batteries was introduced by Surville *et al.* [134] in 1968. In conventional systems, these polymers appear as solid form and include: polyacetylene, polyaniline, polythiophenes, poly(p-phenylene), polyazulene and polyfluorene [135-137]. Among these polymers, polyaniline is commonly used in zinc-based systems due to its high conductivity and stability in aqueous electrolytes [135-137]. However, this kind of batteries suffer from limited specific energy as only the outer layer of the polymer films contribute to the energy storage processes.

To address this issue, Zhao *et al.* [138] proposed the use of polyaniline particles as suspension electrolytes rather than polymer film in a flow cell configuration (See Figure 1). These suspensions were prepared by dispersing the synthesized polyaniline particles in a solution containing zinc and ammonia chloride. The resulting suspension electrolyte was circulated through the flow-cell and appeared as a 'single-flow' system. This is because the liquid electrolyte containing soluble zinc species could penetrate easily through the separators to the negative half-cell compartment through the microporous. In the charge and discharge processes, polyaniline particles undergo doping and dedoping of chloride anions, respectively, with electrochemical behaviours in terms of potentials and current densities similar to that of their film counterpart. Charge-discharge cycling was demonstrated by laboratory scale cell with coulombic efficiency of *c.a.* 97 % at 20 mA cm^{-2} over 30 cycles. The use of current density was significantly higher than those of previous 'film' systems (< 5 mA cm^{-2}). The theoretical energy density of this system (66.5 W h L^{-1}) can be even higher than that of the commercial all-vanadium redox flow batteries [138].

4.2. Positive redox couples involving liquid phase active materials

Liquid-phase positive active materials usually dissolve in electrolytes and appear as soluble species in both oxidized and reduced forms. Similar to conventional redox flow batteries, storage capacities of these electrode reactions can be expanded by increasing the volume and the concentration of the positive electrolytes but still limited by the amount of the zinc electrodeposits at the negative electrode. Unless separator or ion-exchange membrane is used, the charged species could react with metallic zinc electrodeposit and lead to energy loss as a form of self-discharge process. In a few cases, dissolution of zinc electrodeposit is particularly slow in the presence of certain active species at low concentrations, providing a possibility of a membrane-less or single flow configuration. The liquid phase of positive active materials allows the use of porous, three-dimensional electrode materials, which effectively facilitate the positive electrode reactions in terms of reversibility and overpotentials. Although many proposed species are based on low-cost elements, the solubilities (i.e. cerium : *c.a.* 0.8 M, benzoquinone: <0.8 M, ferrocyanide < 1 M) are still lower than that of conventional vanadium electrolytes (*c.a.* 1.5 – 2 M), limiting its energy density for energy storage applications.

4.2.1. Zinc-iron

Early zinc-iron hybrid flow batteries were based on alkaline electrolytes, which was introduced by scientists at Lockheed Missiles and Space Company (LMSC) and known as 'zinc-ferricyanide' since the 1970s [120, 139]. This system is currently commercialized by ViZn Inc. for grid-scale applications [140]. The active materials (zinc and iron) are among the most abundant and the lowest cost metals (< USD$ 4 kg^{-1}) in earth's crust. Ferri- and ferrocyanide are iron complexes known to be highly reversible in alkaline electrolytes. Inorganic ferricyanide is less hazardous than halogen in alkaline but release toxic hydrogen cyanide gas in acidic solutions. The early system was based on solid-state active materials at both charged and discharged states. For the zinc negative electrode reaction, zinc electrodeposit and solid zinc oxides were the charged and discharged products,

respectively. Zincate solution is generated from the solid state zinc oxide during the initial discharge cycle. On the other hand, the active positive materials were ferro- and ferricyanide as forms of precipitates obtained through crystallizers or when the electrolytes reach saturation. Although solid-state active materials were used, the solubility of potassium ferrocyanide in 1 M potassium hydroxide is *c.a.* 0.5 M at 25 °C [120, 121].

In alkaline electrolytes, the half-cell electrode reactions (discharge) are as follows:
At negative electrode:

$$Zn + 4\,OH^- \leftrightarrow Zn(OH)_4{}^{2-} + 2\,e^-\ ,\ E^0 = -1.22\ \text{V}\ \textit{vs.}\ \text{SHE} \tag{14}$$

At positive electrode:

$$Fe(CN)_6{}^{3-} + e^- \leftrightarrow Fe(CN)_6{}^{4-}\ ,\ E^0 = +0.36\ \text{V}\ \textit{vs.}\ \text{SHE} \tag{15}$$

Overall reaction:

$$Zn + 2\,Fe(CN)_6{}^{3-} + 4\,OH^- \leftrightarrow\ Zn(OH)_4{}^{2-} + 2\,Fe(CN)_6{}^{4-}\ ,\ E_{cell} = 1.58\ \text{V} \tag{16}$$

In experimental system, the open-circuit voltage (*c.a.* 1.5 – 1.8 V) was even higher than the predicted values based on standard electrode potentials (1.58 V). The negative electrode was typically a cadmium or silver coated substrate, while nickel plated graphite felt was used as the positive electrode material. Separator or membrane was required to avoid crossover of ferricyanide into the zincate containing negative electrolytes, which would result in undesirable precipitates. For instance, zinc ferrocyanide could electrodeposit an insoluble film at low hydroxide concentration (i.e. < 1 M). Previous experiments show that zinc electrodeposition is the limiting reaction with half-cell coulombic efficiency of *c.a.* 85 %, compared to *c.a.* 97 % obtained at the positive half-cell. This system was reported to have a relatively long cycle life of up to 250 cycles [120, 121]. However, high membrane costs and challenges with handling solid zinc oxide precipitates have been considered as the major hurdle for practising this chemistry. The capacity of zinc negative electrode was still limited to less than less than 500 mA h cm^{-2} [120, 121].

In addition to alkaline systems, a few acidic systems have been recently introduced [141, 142].

In acidic electrolytes, the half-cell electrode reactions (discharge) are as follows:

At negative electrode:

$$Zn \leftrightarrow Zn^{2+} + 2\,e^-\ ,\ E^0 = -0.76\ \text{V}\ \textit{vs.}\ \text{SHE} \tag{17}$$

At positive electrode:

$$Fe^{3+} + e^- \leftrightarrow Fe^{2+}\ ,\ E^0 = +0.77\ \text{V}\ \textit{vs.}\ \text{SHE} \tag{18}$$

Overall reaction:

$$Zn + Fe^{3+} \leftrightarrow Zn^{2+} + Fe^{2+}\ \ ,\ E_{cell} = 1.53\ \text{V} \tag{19}$$

For instance, Xie *et al.* [142] introduced a mixed acid system using 1 M zinc sulphate with 1.5 M sodium acetate and 1.5 M acetic acid as the negative electrolyte, while positive electrolyte contains 1 M iron(II) chloride in 1.5

M sulphuric acid. The resulting cell voltage (1.53 V) is comparable to that of the aforementioned alkaline systems (*c.a.* 1.5 – 1.8 V). It was found that the role of acetate buffer solution is crucial for the battery performance as it controls the concentration of free proton in a preferred range, especially more proton transfers from the positive to the negative half-cell. Furthermore, higher concentration of acid is favourable for the kinetics of the iron(II)/iron(III) reactions. With the addition of such buffer solution, the coulombic efficiency increases from less than 20 % to *c.a.* 91 % at 30 mA cm^{-2}. It is also important to note that carbon felt was also used as the negative electrode, which tends to be difficult to deposit zinc without the buffer solution.

Selverston *et al.* [141] proposed another acidic system by using mixed solutions of zinc and iron species for both negative and positive electrolytes. The pH of the electrolytes was controlled at pH 1 to avoid the formation of insoluble iron hydroxide precipitates, while minimizing the hydrogen evolutions. As long as the galvanic displacement of zinc by iron is low, zinc electrodeposition was carried out instead of iron electrodeposition as a primary reaction at the negative electrode. On the other hand, the zinc ions have no significant effect on the positive iron(II/III) redox reaction at the positive electrode. However, the incorporation of iron was only observed in cases of low zinc concentrations (or high iron concentration) or at high current densities. With the use of Daramic® microporous separator, the energy efficiencies of this system was more than 60 % over 120 cycles at 25 mA cm^{-2}, which shows that the system is crossover-tolerant. Based on this performance and configuration, the estimated cost of a 5.5 h system would be about USD$100 / kWh [141].

In addition to pure alkaline or acidic systems, Gong *et al.* [143] has proposed an alkaline (zinc) – acidic (iron) system to yield a cell voltage as high as 1.99 V. Since the two supporting electrolytes have very different pHs, it is not feasible to use conventional single membrane configuration. Instead, a double-membrane triple-electrolyte configuration was used as illustrated in Figure 8, in which a neutral sodium chloride supporting electrolyte was used in the middle compartment between the two ion-exchange membranes. Nafion® 212/211 (Dupont) and FAA-3 (Fumatech) were used as the cation and anion exchange membranes, respectively. The overall cell resistance was observed to be smaller at higher electrolyte flow rate or with smaller thickness of electrolyte compartment. It was reported that energy efficiencies were more than 50 % at 80 mA cm^{-2} over 20 cycles. Together with its relatively high cell voltage, a peak power density was delivered at 660 mA cm^{-2} at 70 % state of charge. Since protons and hydroxide ions can transfer through the ion-exchange membranes, the pHs of these electrolytes will change in long-term and require periodic adjustment. For this particular system, further work should focus on more selective ion-conductive membranes while ensuring that the cost is significantly lower than their perfluorinated counterparts. (i.e. Nafion®) [143].

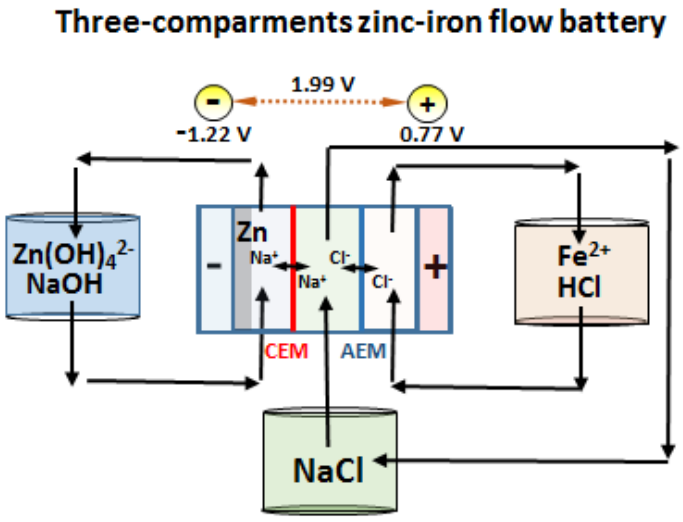

Figure 8. Three-compartments zinc-iron hybrid flow batteries, using $Zn(OH)_4^{2-}/Zn$ as negative redox pair in sodium hydroxide solution, NaCl as middle electrolyte and Fe^{3+}/Fe^{2+} as positive redox pair in hydrochloric acid solution [143].

4.2.2. Zinc-cerium

The zinc-cerium hybrid flow battery was first patented by Clarke *et al*. [144, 145] in 2004 and has been developed by Plurion Inc. [63]. As claimed by this company, a 2 kW system has been installed in their testing facility in Scotland. The proposed system used carbon polymer substrate and platinized carbon/ titanium as the negative and positive electrodes, respectively [144, 145]. Nafion® cation exchange membranes were used to separate the two half-cell compartments. The proposed system make use of methanesulfonic acid as the supporting electrolyte to yield reasonable solubilities of both zinc (> 2 M) and cerium species (*c.a.* 0.8 M) in both oxidized and reduced forms. In contrast, solubilities of cerium species are still too low (< 0.3 M) in sulphate electrolytes for energy storage applications [146].

At positive electrode:

$$Ce^{4+} + e^{-} \leftrightarrow Ce^{3+}\ ,\ E^{0} = +\ 1.28 - 1.72\ \text{V}\ \textit{vs.}\ \text{SHE} \tag{20}$$

Overall reaction:

$$Zn + 2\ Ce^{4+} \leftrightarrow Zn^{2+} + 2\ Ce^{3+}\ ,\ E_{cell} = \text{up to } 2.48\ \text{V} \tag{21}$$

As claimed by Plurion Inc. [144, 145], their batteries operated at 60 ºC and under constant voltage discharge [63]. The discharge current densities were up to 100 mA cm^{-2} with coulombic efficiencies of more than 70 % over 60 cycles. Since the 2010s, the electrochemical information and charge-discharge performance have been evaluated by a number of researchers [54, 86, 89, 147-162]. In the works of Leung *et al*. [86, 89, 147] , a number of two- and three-dimension electrode materials have been evaluated for the cerium redox reactions. In terms of chemical stability and overpotentials, platinized titanium mesh stack electrode was the most suitable for long-term performance. In contrast, carbon-based materials tend to be oxidized in cerium containing electrolytes [147].

Considering the solubility of cerium(III) species is contrary to that of cerium(IV) ion, high methanesulfonic acid concentration (4 M) is required to maintain reasonable solubilities for both cerium(III) and cerium(IV) species (Figure 9). To facilitate efficient zinc electrode reaction, a lower acid concentration (1 M) was used in the negative electrolytes. In typical operations, coulombic and voltage efficiencies were up to 92 % and 68 %, respectively, at 50 mA cm^{-2} and 50 ºC [147]. However, the higher concentration of acid has tendency to transfer towards the negative side through the cation-exchange membranes, which makes zinc electrodeposition more difficult in long-term. Regarding the zinc half-cell study, no significant dendrite formation was observed after 4 h under the same operating conditions. It was reported the use of indium additives could suppress hydrogen evolutions and exhibit lower deposition overpotential, which lead to faster electrodeposition rate and boulder-like agglomerate morphologies [89]. Some common organic and inorganic additives, including cetyl trimethylammonium bromide and lead oxide, tended to inhibit corrosion effectively over a period of time, but their strong blocking effect leads to relatively low half-cell coulombic efficiencies [54, 89].

Following this, a membrane-less system has also been introduced by the same authors making use of relatively slow dissolution of zinc at lower acid concentrations and efficient cerium redox reaction using carbon felt electrodes [148, 149]. The common electrolyte used contained 1.5 M zinc(II) and 0.2 M Ce(III) in 0.5 M methanesulfonic acid. In such configuration, the discharge cell voltage and energy efficiencies were still up to 2.1 V and 75 %, respectively, at 20 mA cm^{-2} and room temperature. The self-discharge process was slow and took up to 7 h after charging for half an hour [148, 149]. To minimize the self-discharge and allow the use of higher cerium concentration at low acid concentration, mixed acid electrolytes have been proposed by a few researchers [149-151]. As shown in the solubility charts (Figure 9a and b), more than 0.5 M cerium species at both oxidizied and reduced forms can be made soluble at low concentrations of methanesulfonic acid and sulfuric acid, respectively [149]. In the work of Xie *et al.* [150], up to 1 M of cerium species can dissolve in a mixed acid of 2 M methanesulfonic acid and 0.5 M sulfuric acid. The use of mixed acid, including chloride also tends to increase the kinetics of cerium species at < 40 ºC [150, 151]. In addition to platinum based electrode, a number of precious

metal-based electrode have been evaluated by Nikiforidis *et al.* [152], in which platinum-iridium based electrodes had the best electrochemical performance. Meanwhile, lower cost materials, including hierarchical porous carbon [153], grapheme oxide [154], tin oxide [155] and indium modified [156] carbon felts, have been observed to have improved reaction kinetics than conventional carbon-based materials. Future work of this system should focus on low-cost, chemically stable electrodes and electrolytes to dissolve more cerium species at low acid concentrations. Electrolyte additives for improving morphologies and inhibiting corrosion of zinc electrodeposits are important for operations at elevated temperature or/and at high acid concentrations.

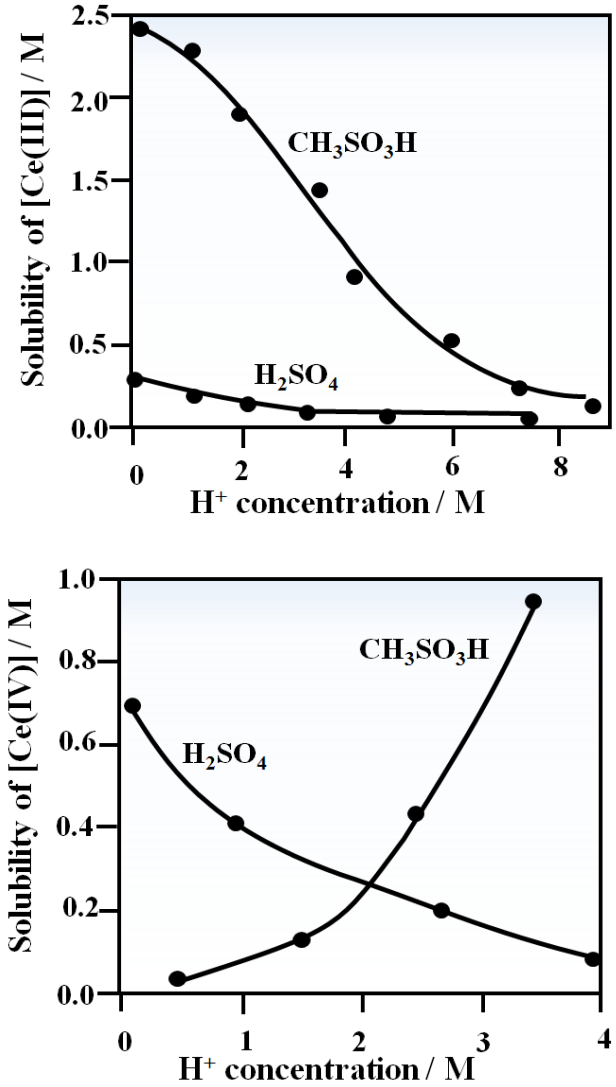

Figure 9. The solubility of (a) Ce(III) and (b) Ce(IV) ions in aqueous methanesulfonic and sulphuric acid electrolytes [149].

4.2.3. Zinc-iodine

The zinc-iodine battery was first described as a primary system by Martin for academic demonstration in 1949 [163], which used metallic zinc and potassium iodide solution as active electrode materials. About a decade later, Jones and Arranaga [164] proposed another primary system using solid iodate instead of liquid iodide solution as the positive active material. Electrical energy was released by mechanically forcing sulphuric acid solutions to

the battery through compressed carbon dioxide gas. Despite relatively large current output (up to 100 mA cm^{-2}), this system is not rechargeable and is based on highly corrosive electrolyte (*c.a.* 4 M sulphuric acid).

Although iodine (I_2) has low solubility, its solubility increases significantly in the presence of iodide (I^-) due to the formation of the polyiodide ions (I_3^-). Since iodide (or triiodide) has high solubilities in aqueous electrolytes (i.e. lithium iodide: *c.a.* 8.2 M; zinc iodide: *c.a.* 5.6 M), it has been considered as an attractive redox couple for flow battery applications [165]. Following the introduction of lithium-iodide system (2013), a zinc-iodide flow battery has been developed by Li *et al*. [165] in 2015.

The overall electrode reactions are as follows:

At positive electrode:

$$I_3^- + 2e^- \leftrightarrow 3I^- \text{ , } E^0 = 0.54 \text{ V } vs. \text{ SHE} \quad (22)$$

Overall reaction:

$$I_3^- + Zn \leftrightarrow 3I^- + Zn^{2+} \text{ , } E_{cell} = 1.30 \text{ V} \quad (23)$$

Both negative and positive electrolytes are based on zinc iodide salt (ZnI_2) in water. It is important to note that no acid or alkaline is added in the electrolytes, resulting in a nearly neutral electrolyte (pH 3 – 4) at 0 % state-of-charge. The flow cell has been charge-discharge cycled in a range of current densities between 5 and 20 mA cm^{-2}. The energy efficiencies decreased from *c.a.* 91 % to *c.a.* 76 % as the concentration of zinc iodide increases from 0.5 to 3.5 M, which is attributed to the increasing electrolyte resistances at concentrated electrolytes. A maximum positive electrolyte energy density of 167 W h L^{-1} (compared to 20 – 35 W h L^{-1} of conventional vanadium electrolytes). It was also found that the addition of ethanol could induce ligand formation between oxygen on the hydroxyl groups and zinc ions, further expanding the electrolyte window to from – 20 to 50 °C [165].

Following this, Weng *et al.*[166] proposed the use of bromide ions (Br^-) as a complexing agent to stabilize the free iodine by forming iodine-bromide ions (I_2Br^-) as a mean to free up iodate ions, hence enabling higher discharge capacity of positive electrolyte. Compared to chloride ions, bromide ions tend to be more stable and exhibit less hydrolysis issues. As shown in Figure 10, both centrosymmetric I_3^- and asymmetric I_2Br^- tend to have linear (or nearly linear) trihalide structure, which are thermodynamically stable. With the use of bromide ions, the capacity of positive electrolyte was up to 202 Wh L^{-1}, which is among the highest energy density achieved for aqueous flow battery to date. To improve the reaction kinetics and avoid the use of expensive catalysts, porous coordination polymers were proposed by Li *et al.* [167] as a catalyst for the positive iodide reaction. [6]. Nevertheless, poor chemical stability of this material, especially under electrolyte soaking, is a major challenge for future applications. Despite the high solubilities of the iodide redox species, the overall capacity of this battery is still limited by the zinc negative electrode. Since the same electrolyte is used for both half-cells, further cost reduction can be possible with the development of low-cost separators.

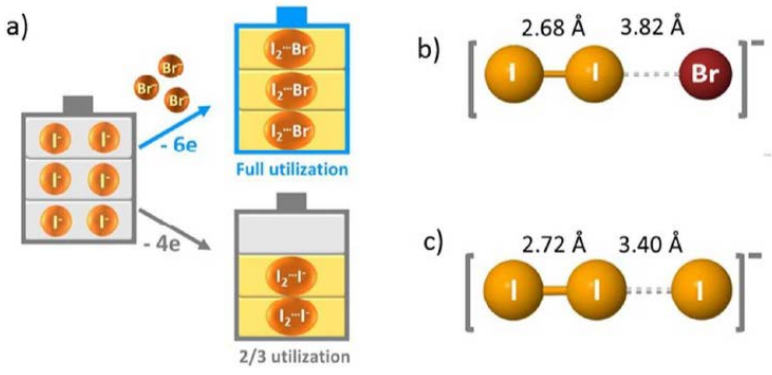

Figure 10. Concept illustration of bromide as the complexing agent to stabilize iodine. b, Structure of I_2Br^- ion. c, Structure of I_3^- ion. *The bonding length is obtained from the first-principles density functional theory calculations [166]..

4.2.4. Zinc-polymer (dissolved)

In addition to polymer suspensions described in Section 4.1.3., the use of organic polymers have become popular in the field of aqueous organic redox flow batteries. As proposed by Janoschka *et al*. in 2012 [168], these organic polymers typically dissolve in electrolytes and consist of two parts, namely a redox active moiety and an unit providing sufficient aqueous solubility to prevent precipitation [169-171]. The same research group [172] made use of this kind of polymer and introduced an organic-inorganic system by coupling with zinc anode. The early proposed system used aqueous electrolytes based on chloride salts. Zinc chloride not only serves as the active species but also as the supporting electrolytes. Poly(ethylene glycol) methyl ether methacrylate (PEGMA) and [2-(methacryloyloxy)ethyl]trimethylammonium chloride (METAC) were used as the copolymer of the active material, which was 2,2,6,6-tetramethylpiperidinyl-*N*-oxyl (TEMPO) in that study [172].

In flow cell studies, microporous separator was used to prevent the crossover of such polymer active materials, while porous carbon papers or felts were used as electrode materials for both half-cell reactions. With these organic polymers, the open-circuit cell voltages were more than 1.2 V. Compared to METAC-based polymeric TEMPO, PEGMA-based polymers have higher solubilities and do not precipitate in concentrated zinc chloride electrolytes (1 M). In such electrolytes, the capacities of up to *c.a.* 2.4 was achieved and decreased linearly with higher current densities. In static cells, the coulombic and energy efficiencies were over 80 % and 50 %, respectively, at 3 mA cm^{-2} [172].

In these aqueous systems, the current densities were still limited to less 20 mA cm^{-2}. The same research group proposed another similar system based on polymeric-TEMPO in non-aqueous electrolytes [173]. Instead of using regular, linear polymers, this work used well-defined TEMPO-methacrylate/styrene block copolymers (PTMA-*b*-PS) featuring miscellar structures. Mixtures of carbonate electrolytes were used for both negative and positive electrolytes. The maximum concentrations for the organic polymer were up to 13 mg cm^{-3} in the positive electrolytes. Similar to the aforementioned aqueous systems, the charge-discharge capacities decreased linearly with higher current densities but with lower current density range (< 5 mA cm^{-2}). The coulombic efficiencies were more than 90 % over a range of current densities (0.5 – 5 mA cm^{-2}). With suitable cell architectures and selections of components (i.e. separators), improved current densities of more than 35 mA cm^{-2} have been demonstrated in other similar works using aqueous and non-aqueous electrolytes [7, 8].

4.2.5. Zinc-organic (non-polymer)

As discussed in Section 4.2.4, polymer is a kind of organic material and has been used in a number of zinc-based batteries [136-138]. To distinguish the polymer system, this section focused on the particular use of soluble organic materials for zinc-based flow batteries. The first few metal-organic hybrid flow batteries were introduced by Xu *et al.* [9, 174] in 2009. The initial systems used cadmium and lead as the negative electrodes, which are less negative (–0.42 V vs. SHE) than zinc (–0.76 V *vs.* SHE) in aqueous electrolytes, implying that zinc-based systems are even more attractive in terms of cell voltages and cost. On the other hand, derivatives of quinone and 2,2,6,6,-tetramethylpiperidinyloxyl (TEMPO) based materials, are the most studied positive redox couples in the recent development of organic-based flow batteries [7, 8]. Many of these molecules exhibit relatively positive redox potentials (> 0.5 V vs. SHE), high solubilities in aqueous electrolytes (> 0.5 M) and commercially available at low-cost. Unlike many other organic active materials, the chemical structures of these molecules enable long-term stability and are suitable for energy storage applications.

In 2016, Orita *et al*. [175] proposed a zinc-organic hybrid flow battery based on soluble TEMPO derivatives by functionalizing with a hydroxyl group. The charge-discharge reactions of the proposed system are as follows:

At positive electrode:

$$TEMPO^{+} + \ e^{-} \leftrightarrow \ TEMPO \ , E^{0} = + 0.83 \text{ V } \textit{vs.} \text{ SHE} \quad (24)$$

Overall reaction:

$$Zn + 2\,TEMPO^{+} \leftrightarrow Zn^{2+} + \ 2\,TEMPO \ , E_{cell} = 1.59 \text{ V} \quad (25)$$

The resulting hydroxyl-TEMPO has ability to dissolve at concentrations as high as 3.6 M. The proposed system used metallic zinc and carbon felts as the negative and positive electrode materials, respectively. Both cation (Nafion® 212) and anion exchange membranes (Selemion DSV) were tested in two different supporting electrolytes (1 M sodium perchlorate or sodium chloride). In all cases, the open-circuit cell voltages were more than 1.6 V upon charging. The energy efficiencies were the highest (80.4 %) at 10 mA cm^{-2}, when Nafion® 212 membrane and sodium perchlorate electrolytes were used. The capacity of the resulting battery tended to decrease after cycles. This is attributed to the decrease in hydroxyl-TEMPO concentration caused by its side reaction, which convert the active materials into other organic molecules. Charge-discharge cycling was also performed at high hydroxyl-TEMPO concentration (1 M), the initial energy efficiencies were lower (67. 5 %) at 10 mA cm^{-2}. The discharge capacity and energy densities were 8 A h L^{-1} and 9.6 W h L^{-1}, respectively. However, the capacity retention dropped rapidly to 0 % within 5 cycles, possibly due to the chemical degradation of active materials in the presence of the generated hydroxyl ions. For these reasons, stable control of electrolytes and long-term stability of active materials are necessary for improved battery performances [175].

In the same year, membrane-less zinc organic hybrid flow battery was introduced by Leung *et al.* [58, 59]. The operating concept makes use of the slow dissolution of zinc electrodeposit in the presence of soluble benzoquinone species at low concentrations (*c.a.* 0.1 M) in the common electrolytes. Instead of prototypical 1,4-hydroquinone, 1,2-hydroquinone-disulfonic acid was used due to more redox potentials (+0.85 V *vs.* SHE), resulting in a cell voltage of more than 1.4 V. Unlike the aforementioned TEMPO derived species, both negative and positive electrode reactions undergo two-electron-transfers processes. Despite relatively low current densities (30 mA cm^{-2}), the capital cost of this system is still lower than the cost target (USD$150 /kW h by the US Department of Energy in long-term, while electrolyte cost is just USD$ 14 /kW h or less. In the absence of separator, the charged species are free to react with the zinc electrodeposit as a self-discharge process. The corrosion current densities were estimated to be less than 10 mA cm^{-2}, which is still lower than the current densities used (30 mA cm^{-2}) [58, 59].

At positive electrode:

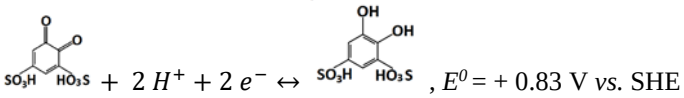

(26)

Overall reaction:

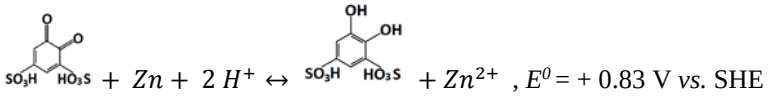

(27)

With the use of single flow configuration, carbon substrate and felt were used as the negative and positive electrodes, respectively. Concentrated zinc species (1.5 M) was used in the common electrolyte to facilitate the zinc elecrodeposition process and avoid mass transport limitation. The battery was charge-discharge cycled with an average energy efficiency of *ca.* 73 % at 30 mA cm^{-2} for more than 12 cycles. The low concentration of the

organic species (50 mM) implies a relatively low specific energy compared to conventional systems, although its cost advantage is still maintained. To further minimize the capital cost per kW h, future work should focus on the use of higher current densities, facilitated by improved mass transport and cell architecture. Higher specific energy can be achieved at higher organic active species concentrations with the use of separator, which tends to add further cost to the system [58, 59].

4.3. Positive redox couples involving gaseous phase active materials

In some zinc-based hybrid flow batteries, gaseous active materials, particularly oxygen and halogen (i.e. bromine, chlorine), are often generated in the positive electrode reactions during the charging processes. Compared to halogen, oxygen as a charged species is not hazardous to human and is continuously supplied from atmospheric air. For these reasons, there is no specific requirement in gas storage, resulting in simplified cell design. Despite relatively large overpotentials, bifunctional catalysts enable both reduction and oxidation reactions to take place at the same electrode. Since oxygen (as the charged species) is negligible in the electrolytes, no separator or ion-exchange membrane is required, resulting as a membrane-less or single flow system.

In contrast, bromine and chlorine are harmful gases evolved in the charging processes. These gases species are often sequestered or condensed into liquid or solid phases (i.e. forming polybromide in oily phase; forming solid chlorine hydrate with water at 10 ^{o}C) and stored carefully in specific chambers. Upon discharge, these halogen species are often mixed with the zinc containing solutions and pass through the porous electrode within the positive half-cells. In typical cases, these halogen species are corrosive to metallic electrodeposits. Therefore, separator or ion-exchange membrane are often used to prevent the permeation of these species towards the negative half-cell and ensure high coulombic efficiencies.

4.3.1. Zinc-air

The zinc-air battery was originally developed as primary batteries in the 1930s [176] based on the concept of Leclanché wet cells (zinc-manganese dioxide, 1866) [13]. Since the 1970s, mechanically rechargeable system were introduced without the electrochemical charging process [177], spent zinc metal is physically replaced with fresh anodes, or refueled as a form of zinc slurry by pump [178, 179]. Rechargeable systems by mean of electrochemical approach has become available with the developments of bifunctional catalysts for the oxygen evolution and reduction reactions, which are based on low-cost and sometimes non-metal materials [180, 181]. In all these cases, alkaline electrolytes are used due to the higher activity of both zinc and air electrode reactions:

At negative electrode:

$$Zn + 4\,OH^- \leftrightarrow Zn(OH)_4{}^{2-} + 2\,e^- \text{ , } E^0 = -1.22 \text{ V } \textit{vs.} \text{ SHE} \quad (28)$$

$$Zn(OH)_4{}^{2-} \leftrightarrow ZnO + H_2O + 2\,OH^- \quad (29)$$

At positive electrode:

$$O_2 + 4\,e^- + 2\,H_2O \leftrightarrow 4\,OH^- \text{ , } E^0 = +0.4 \text{ V } \textit{vs.} \text{ SHE} \quad (30)$$

Overall reaction:

$$2Zn + O_2 \leftrightarrow 2\,ZnO \text{ , } E_{cell} = 1.62 \text{ V} \quad (31)$$

In practice, the working cell voltage of primary systems is typically 1.0 – 1.4 V, lower than the standard potential (1.62 V), under considerable current densities (up to 100 mA cm^{-2}) [181]. This kind of batteries have been implemented for medical and telecommunication applications [182]. For rechargeable system, a large charge

voltage of 2 V or higher have been observed due to the substantial overpotentials of the positive oxygen electrode reactions, restricting the current densities to be lower than 30 mA cm^{-2} [181]. These systems have advantages in terms of flat discharge voltage, safety, low-cost and low self-discharge rate. However, extended cycle life and long discharge duration have been troubled by non-uniform zinc electrodeposition and lack of durable bifunctional catalysts.

To improve the morphologies and avoid the dendritic growth, flowing electrolyte has been used in zinc-air rechargeable batteries. The early system was introduced by Lawrence Berkeley Laboratory [183, 184] in 1988. Unlike conventional zinc-air systems using granular powder or pellets (as a gelled mixture), the flow system stores energy through electrodeposition of zinc. The proposed system (2 W) used porous reticulated carbon and bifunctional air catalyst as the negative and positive electrodes, respectively. Unlike other flow systems, no membrane or separator is necessarily required. In the zinc negative half-cell, no apparent shape change or dendritic growth were observed over 600 cycles with a discharge capacity of *c.a.* 200 mA h cm^{-2}. The specific energy was estimated to be 110 Wh kg^{-1}, which was compared to other zinc-air rechargeable systems at large-scale [185]. Considering most materials are inexpensive, the cost of this system was estimated to be as low as USD$ 20 / kW h (at 1980's value) [120], which is still believe to be lower cost than other zinc-based systems.

After a few decades, similar system was introduced by Pan *et al.* [186] using the concept of single flow system. A composite electrode was used as the positive electrode, one side of this electrode facing the aqueous electrolyte used nano-structured $Ni(OH)_2$ for the evolution reaction, while the other side facing atmospheric air used MnO_2 doped with $NaBiO_3$ catalysts for the reduction process. At 20 mA cm^{-2} and 60 °C, the charge and discharge voltages were 1.78 V and 1.32 V, respectively. By circulating the electrolytes, dendritic growth and shape change of the zinc negative electrode has been effectively prevented. It was also shown that energy efficiencies of more than 70 % were obtained over 150 cycles.

Considering significant energy is consumed during oxygen evolution, Wen *et al.* [187] proposed a dual functional system to use this energy to generate organic acid instead through another positive half-cell, in which raw materials are continuously supplied through circulation as shown in Figure 11. Organic acids, such as propanoic acid, glyoxylic acid and cysterici acid, are oxidized from raw materials of propanol, glyoxyal and xysteine, respectively. A common negative electrode was shared with the two positive half-cells. In the charging process, propanol is oxidized to propanoic acid and zinc is electrodeposited at the negative electrode. During discharge, oxygen is reduced at the other positive electrode and metallic zinc dissolutes back to the electrolyte to release energy. The energy efficiency of the battery is up to *c.a.* 59 %, which means that percentage of energy consumed by the organic electro-synthesis can be recovered. The other work of the same authors [188] also reported that spongy morphologies can be suppressed effectively with lead and tungstate ions, although co-electrodeposition of lead and zinc ions may occur. Similar to most alkaline zinc-based batteries, challenges of dendritic growth, zinc oxide precipitation, shape change of electrodes need to be further addressed. The overpotential of the positive electrode reaction needs to be minimized with the development of low-cost and durable catalysts. Improved cell design or architecture is important to ensure efficient oxygen transfer to a number of cells within a stack system.

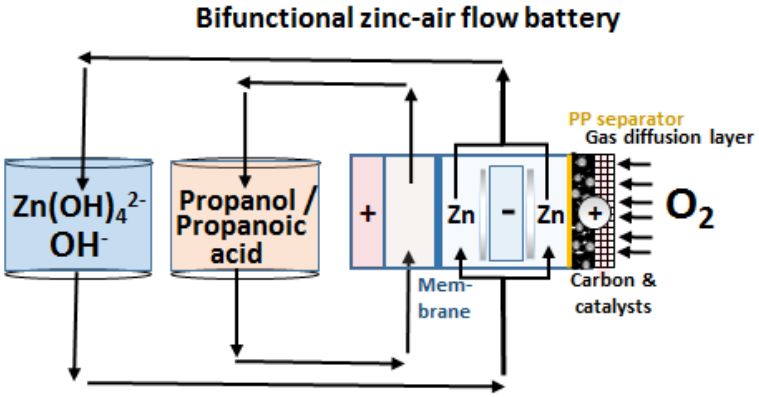

Figure 11. Bifunctional zinc-air hybrid flow batteries by using propanol oxidation as a counter electrode reaction [187].

4.3.2. Zinc-bromine

The zinc-bromine battery was first patented in 1885[189] and has been developed as hybrid flow battery by Exxon, Gould and National Aeronautics and Space Administration (NASA) in the 1970s [190]. This kind of battery has high theoretical energy density (440 W h kg^{-1}) and cell voltages (*c.a.* 1.8 V). Over the past few decades, the zinc-bromine hybrid flow batteries have been commercialized and installed by several companies (See Section 6). The specific energy of these commercial system is still limited to 60 – 85 Wh kg^{-1} [191], which is just 20 % of the theoretical value. In flow cell configuration, zinc bromine electrolytes are circulated in both half-cells through external pumps. In the positive electrolyte, a quaternary bromide salt (QBr), such as N-methyl N-ethyl pyrrolidinium bromide (MEP) or N-methyl N-ethyl morpholinium bromide (MEM), is added as a sequestering/ complexing agent [192, 193] to sequester the evolved bromine into an alternate phase with low vapour pressure in the charging process. The sequestered bromine is then stored in an oily phase that remains separated from the main aqueous phase due to the higher specific gravity of these complexed phase. The concentration ratio of QBr to $ZnBr_2$ is typically 1:3 [194, 195], which means 1 M of sequestering agent is used with 3 M zinc bromine solutions.

The overall electrode reactions can be described as follows:
At positive electrode:

$$Br_2 + 2e^- \leftrightarrow 2Br^- \; E^0 = +1.087 \text{ V } \textit{vs.} \text{ SHE} \tag{32}$$

Overall reaction:

$$Br_2 + Zn \leftrightarrow 2Br^- + Zn^{2+} \text{ , } E_{cell} = 1.849 \text{ V} \tag{33}$$

The actual chemical species are even much more complicated as complexing agents are added to form polybromide ions (Br_n^-; n = 3, 5, 7), which tends to be more sluggish due to the addition of an additional sequestration/ dissociation steps during the charge-discharge processes. The overpotentials of both electrode reactions are relatively low (< 200 mV at 100 mA cm^{-2}) and usually larger for the zinc negative electrode reactions due to the use of planar electrodes [196]. As reported by Lim *et al*. [196], formations of dendrites are often observed when the current densities were as low as *c.a.* 15 mA cm^{-2}, although prolonged charge (i.e. 10 h) has been demonstrated.

For commercial systems, the operating pH range is relatively narrow (between 1 and 3.5) and needs to be controlled throughout the operations. For instance, undesirable mossy morphology and bromate formation tend to take place above pH 3. When the pH is higher than 6, solid zinc oxide is formed rather than soluble Zn^{2+} species ($ZnBr_3^-$) as suggested by the relevant Pourbaix diagram [191]. At lower pHs, corrosion and hydrogen evolution become more dominant and lead to lower coulombic efficiencies [196]. When the pH is lower than 1, excessive hydrogen evolution was observed and resulted in higher overpotential due to the trapping of gas bubbles on the surfaces of the electrodes [196] .

The influence of supporting electrolytes regarding electrode reactions[197, 198], solubilities and ionic conductivities [196, 199] have been evaluated under a wide range of salts (Na^+, NH_4^+, Cl^-, Br^-, SO_4^{2-}, $H_2PO_4^-$ and NO_3^-). Chloride based electrolytes (up to 0.5 M) tend to perform poorer than their sulphate, bromide or phosphate counterparts, while nitrate electrolyte is not suitable. However, the ligands of zinc complexes could affect the electrochemical performance of the half-cell electrode reactions [198]. The addition of bromine sequestration agents (i.e. MEP, MEM) exhibit higher reversibility in terms of anodic to cathodic current ratios in the cyclic voltammograms as shown in Figure 12, which is due to the aggregation and effective complexation with bromine [192].

Similar to other hybrid flow batteries, shunt current causes uneven electrodeposition in each unit cell and results in lower discharge capacity [63, 200]. This can be minimized by appropriate cell designs with feed channels to each cell long and narrow enough to increase the electrical resistance. To improve the morphology of zinc electrodeposits, organic [201, 202] and inorganic additives [203] have been added to the electrolytes. In some cases, the ionic liquid additives used for bromine sequestration [201, 204] and inorganic salts, i.e. zinc perchlorate [63], were observed to reduce the crystal size and prevent dendritic formation. Surface active agents are known to suppress zinc dendrites but also promote mixing of the aqueous and polybomide phases, enabling the bromine reaction to take place evenly on the electrode surface [202]. Poor mixing of the polybromide-complex phase (particularly at the bottom of the cell) is commonly observed in the zinc-bromine flow batteries [202].

For bromine positive electrode reactions, three-dimensional carbon based materials, mainly carbon felts [192, 205] and reticulated vitreous carbon [196, 206], have been used in typical systems to facilitate the bromine reactions by minimizing the overpotentials. Recent investigations have further enhanced the reaction kinetics by developing electrode materials with high activity, such as carbon nanotubes [205, 207], active carbon [208] and carbon black [209, 210]. Other approaches include surface modifications [208, 211] and electrochemical exfoliation, such as halogenation [212]. Some of these systems have been demonstrated to operate at current density as high as 80 mA cm^{-2} with energy efficiency of *c.a.* 80 % [210].

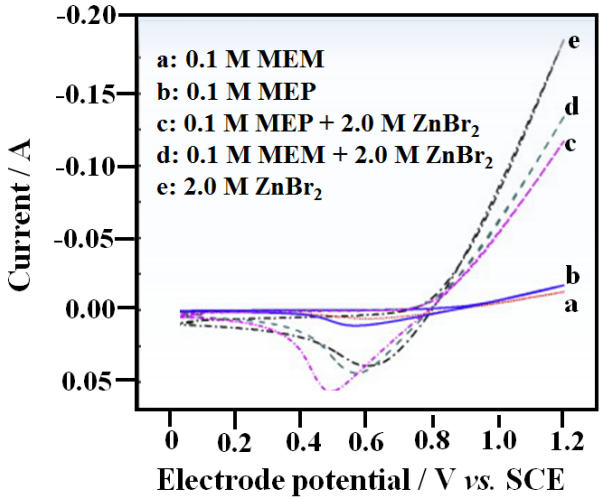

Figure 12. Infleunce of bromine sequestration agents (MEP, MEM) on zinc-bromine electrolytes (2 M Zn^{2+}, pH 3, at 20 mV s^{-1} and 25 ^{o}C.

Despite the low-cost active materials (zinc and bromine), the overall cost of zinc-bromine system is not necessarily lower than commercial all-vanadium redox flow batteries [191], which is attributed to the use of expensive sequestering/ complexing agents and the relatively low current density of the systems (< 50 mA cm^{-2}, implying more cells are required for equivalent power output). To improve the energy density, a single flow cell system has been demonstrated, in which carbon felt electrodes were coated with active materials and sealed within the compartment to avoid bromine emissions as shown in Figure 1 [192]. Other recent system also demonstrate reasonable performance (energy efficiency of *c.a.* 74 % at 40 mA cm^{-2}) in the absence of such sequestering agents [197]. Improved cell architecture and electrolyte circulations could further improve the morphologies of zinc electrodeposition and avoid poor mixing of polybromine and aqueous phases [213]. To-date, specific energy of the commercial system (60 – 85 Wh kg^{-1}) still requires significant improvement, which is currently less than 20 % of their theoretical value (440 Wh kg^{-1}) [191]. Future research directions should focus on approaches to improve the energy density and cell performance at lower-cost by mean of cell designs and material developments.

4.3.3. Zinc-chlorine

The zinc-chlorine battery was introduced by Charles Renard in 1884 [214]. Further development of this technology has been made by Energy Development Association Inc. (EDA) in the 1970s [215]. The system was developed as a form of flow battery and exhibit relatively high cell voltage of 2.12 V. The overall electrode reactions are described as follows:
At positive electrode:

$$Cl_2 + 2e^- \leftrightarrow 2Cl^- \; E^0 = +1.36\text{V } \textit{vs.}\text{ SHE} \tag{34}$$

Overall reaction:

$$Cl_2 + Zn \leftrightarrow ZnCl_2 \; , E_{cell} = 2.12\text{ V} \tag{35}$$

In the charging process, chlorine gas is evolved at the positive electrode and stored in another chamber by mixing with water to form solid chlorine hydrate at *c.a.* 10 °C. When the battery undergoes a discharge process, chlorine is later reduced back to soluble species. A 10 kW (50 kW h) system has been tested with an energy efficiency of *c.a*. 60 % [215] and cycle life of up to 500 – 5000 cycles [216].

Among early studies, Jorne *et al.* [217] evaluated the half-cell overpotentials of a similar hybrid flow battery, in which graphite plate and porous graphite were used as the negative and positive electrodes, respectively. The two electrodes have active area of 68 cm^2 and gap in between of 0.2 cm. The electrolyte was 2 M zinc chloride solution and circulated at 0.06 L min^{-1}. Despite the use of porous electrodes, the overpotential was mainly observed on the chlorine positive electrode. The overpotentials for charge and discharge processes were +120 mV and –200 mV, respectively. This was mainly caused by the slow kinetics and ohmic losses within the porous structure. The ohmic resistance can be reduced by adding potassium chloride salts. On the other hand, the overpotential of zinc negative electrode reaction was relatively small (< 50 mV) in both charge-discharge processes. The voltage and columbic efficiencies are 78 and 84 %, respectively with an energy efficiency of approximately 66% [217].

The resulting zinc-chlorine hybrid flow battery has a practical energy density of 154 Wh kg^{-1}, higher than that of the similar zinc-bromine systems (60 – 85 Wh kg^{-1}). Since the system requires additional chambers, the estimated cost was about USD$500 – 750 / kW h, significantly higher than the DoE cost target (USD$ 150 / kW h) [216]. Energy loss was attributed to the inefficient processes of hydrogen evolution and dissolving chlorine at the negative and positive electrodes, respectively, in the charging process. Other side reactions include the slow oxidation of graphite by the corrosive chlorine gas, although the electrode life is often expected to exceed the goal of 10 years [215]. Future research direction should focus on safer and more efficient chlorine gas storage as well as more durable electrode materials for long-term operations.

5. Research issues associated with the operating conditions

More detailed investigations on both negative and positive electrode reactions are essential to obtain improved charge-discharge performance for further developments. Attentions should be given to technical issues associated with operating parameters (current density, temperature) and the half-cell chemistries (pH, ligand chemistry, hydrogen evolution and corrosion), which are essential to enable full commercial potential and deep market penetration.

5.1. pH

Electrolyte pH is a crucial factor determining the forms and the reaction mechanisms of the dissolved species as well as their solubilities, conductivities and electrode potentials. Under certain conditions, the relationship between electrode potentials, pHs and the forms of dissolved species have been established in Pourbaix diagrams. Side reactions are also often influenced by the acid or alkaline contents of the electrolytes. For instance, higher acid concentrations tend to promote and suppress hydrogen and oxygen evolutions, respectively [89, 147, 218]. However, these gaseous reactions also consume protons or hydroxide themselves, leading to further changes of the pH in the solutions.

Taking into account that many systems employ ion-exchange membrane (i.e. cation, anion, filtration), proton or hydroxide ion transfers between the two half-cells to balance the reactions depending on the types of these membranes. When proton-exchange membrane (i.e. Nafion®) is used in acidic solution, protons move from the positive half-cell to its negative counterpart to form acid by complexing with the anions during the zinc electrodeposition process (reduction of Zn^{2+} to Zn^{0}). Therefore, acidity or alkalinity changes are almost inevitable in the battery processes.

The increase in acid concentration is known to be undesirable for the zinc negative electrode reactions in terms of electrodeposition and corrosion processes. Buffer solution, such as acetate, has been used in some acidic systems to control the concentration of free proton in a preferred range [142]. In the case of zinc-bromine batteries, a narrow range of pH between 1 and 3.5 is required to maintain throughout the operation [219]. For some positive active species, such as cerium, the influence of particular acid on the solubility of the oxidizied species can be contrary to that on the reduced species. Therefore, a high acid concentration (up to > 3 M) is required to dissolve a modest concentration of active species (i.e. 0.8 M). The potential transfer of this amount of acid through the membrane implies difficulties in the zinc electrodeposition process. At high acid concentration, low current efficiency of zinc electrode reaction is expected due to excessive hydrogen evolution and electrodeposit corrosion in the charge [220] and discharge processes [54], respectively. In general, hydrogen evolution can be observed at low pH (pH < 3) but become excessive when the pH is below 1 [221]. In contrast, high pH may lead to precipitate of $Zn(OH)_2$ layer and result in low current efficiency [222]. pH buffers may be used to stabilize the pH in the electrolytes [223].

5.2. Ligand chemistry

For both negative and positive electrode reactions, redox species dissolved in the electrolytes often appear as coordinated ion forms, although some of them are of mixed stability. At different pH and electrolyte compositions, metal ions often appear at different forms as metal complexes. As suggested by the Pourbaix diagrams, the reactions and the corresponding potentials can be different from each other at different pHs and electrolyte compositions For some complexes, the reactions may take several steps to achieve equilibrium. The whole reaction rate can be changed if one of these reaction steps have been affected.

The stability constants of various metal chelates and those of the anions are summarized elsewhere [107, 224, 225]. These values are associated with dissociation constants, which are highly related to the solubilities of certain species. For those complex ions with low stability constants, such as chloride, tend to have higher solubilities than their sulphate counterparts. Electrode reactions may take place at lower electrode overpotentials and improved reaction kinetics due to weaker ligands. Therefore, electrolytes with mixed anions may further improve the reaction kinetics and solublilities of soluble active species [226-229].

For zinc electrodeposition, it is generally easier to deposit on the substrate surface from these complexes with higher deposition rates and current efficiencies. As discussed in Sections 2 and 3, the low deposition overpotential tends to give poor brightening and leveling performance, therefore suitable additives or complexing agents should be added in the electrolytes [230]. In contrast, despite improved morphologies for those with higher stability constants, the process tends to be less efficient in terms of current efficiencies, especially at low ion concentrations.

5.3. Current density

In zinc-based hybrid flow batteries, negative and positive electrode reactions tend to take place under mixed control due to the distribution of current, potential and electrolyte flow, although it is ideal to avoid mass transport limitation by taking place under charge-transfer controlled. For soluble redox couples involving liquid phase reaction, this can be easily achieved by reducing the local current densities with the uses of high-surface-area or porous electrodes instead of a flat, planar electrodes.

Depending on the available active areas of these materials, higher current outputs are often expected, compared to planar (or two-dimensional) electrode materials. Previous works demonstrate that current densities of typical porous or three-dimensional materials, such as carbon felts and carbon papers, could reach up to more than 200 mA cm^{-2} for liquid-phase reactions (i.e. vanadium and cerium redox reactions) by minimizing the cell resistances with suitable cell architectures and membrane selections [229, 231, 232].

However, the current densities used in most zinc-based systems are usually less than 50 mA cm^{-2}, as restricted by the areas allowed for zinc electrodeposition at the negative electrodes. A few high-surface-area electrodes, such as carbon felts and nickel foams, have been used in zinc hybrid flow battery under acidic and alkaline conditions batteries [116, 142]. It was demonstrated that reasonable energy efficiencies (i.e. > 50 %) can be achieved at ultra-high current densities of up to 300 mA cm^{-2} [116]. Compared to planar surface, it is often much more difficult to electrodeposit zinc in porous structures [142, 221]. This is possibly due to the requirements of high overpotentials for uniform electrodeposition as characterized by 'throwing power' – the ability of electrodeposition into low current density areas as in the areas of high current densities.

Among common zinc electrolytes used in the electroplating industry, the throwing power under a standard condition is of the following order: high cyanide> low cyanide> acid> alkaline non-cycanide [233]. However, the current efficiencies of these electrolytes are often higher than 80 % at low current densities (< 20 mA cm^{-2}). At low current densities (< 20 mA cm^{-2}), the current efficiencies are often higher than 80 % in all these baths as shown in Figure 13, in which acidic baths tend to have higher current efficiencies than their alkaline counterparts. However, early work reported that dendrite-free zinc can be electrodeposited well into the porous reticulated vitreous carbon foam at 100 mA cm^{-2} with the essential uses of organic additives and flowing electrolytes [234].

In existing literatures, zinc electrodeposition was mainly carried out at flat, planar electrodes. In some electrolytes, dendritic growths are observed when the current densities are higher than 15 mA cm^{-2} [196]. At increased current densities, 'burned' coating can be observed when the supply rate of zinc ions to the cathode surface is insufficient to maintain the electrodeposition rate. This phenomenon can be avoided by increasing the zinc(II) ion concentrations and the limiting current densities through convective mass transport control [235]. In some extreme cases, ultra-high current densities of up to 1300 mA cm^{-2} have been reported with the use of very high electrolyte flow rates (up to 5 m s^{-1}) [236].

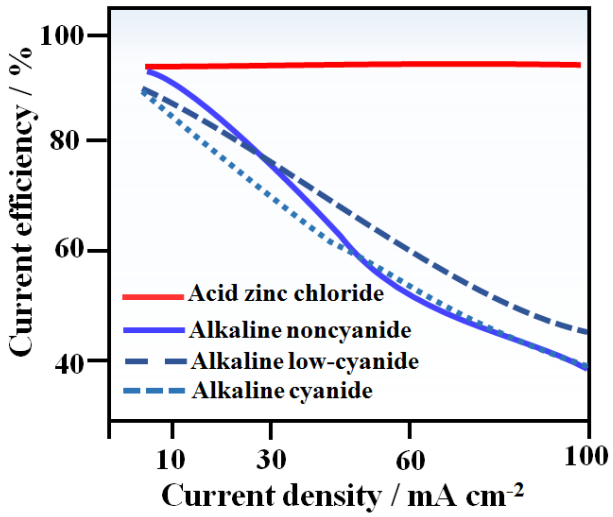

Figure 13. Comparisons of half-cell coulombic efficiency of zinc electrodepositions in acidic and alkaline electrolytes [233].

When the current density increases from 30 to 500 mA cm^{-2}, the surface morphology changes from hexagonal platelets and ridges to the pyridmidal texture in acidic sulphate solutions [237]. However, increased current densities often lead to lower current efficiencies caused by side reactions in both acidic and alkaline electrolytes

[238, 239]. When the current densities are too small, electrodeposition rates may be too slow to form any coating but generally bright electrodeposits are often obtained [240, 241]. In practical systems, zinc electrodepositions in acidic and alkaline electrolytes have been demonstrated with reasonable efficiencies in parallel plate flow cells at 15 – 50 mA cm^{-2} for prolonged charge and discharge processes (charge duration of up to 20 h) [147, 186, 196].

5.4. Temperature

Temperature has influences on both electrode potentials, electrolyte solubilities, electrolyte resistances, reaction kinetics and the diffusion co-efficient of the active species. For zinc-based flow batteries, it is often difficult to define the optimum temperatures for both negative and positive electrode reactions, which vary significantly among different operating parameters (i.e. current densities) and electrolyte compositions (pHs and salts). In both acidic and alkaline solutions, negative zinc electrode reactions tend to be reversible and exhibit high current efficiencies (> 85 %) at low current densities (*c.a.* 20 mA cm^{-2} and ambient temperatures [35, 86, 200, 233]. The influence of temperatures on zinc electrodeposition tends to vary significantly from different literatures [86, 242-246]. In both acidic and alkaline electrolytes, there are some works reported with high coulombic efficiencies observed at elevated temperatures [242-245], while some reported the opposite results due to the stronger depolarizing effect on hydrogen evolution [86, 246] and faster corrosion rates [54]. At elevated temperatures, additive adsorptions and polarizations tend to become weaker. In some cases, additives may loose their functions and become insoluble in the electrolytes [247], leading to poorer efficiency, deposit adherence and morphology [246].

In practice, the influence of temperature should take into account of the positive electrode reactions. For instance, the positive cerium reaction tends to be more sluggish process and appear as the limiting reaction of the full battery at low temperatures (< 50 °C). Together with the limited areas of platinised titanium mesh (compared to high-surface-area carbon felts), the half-cell coulombic efficiency of cerium reaction was even lower than 50 % at 25 °C. As suggested by fundamental studies [89], elevated temperatures (50 °C) effectively improve the reversibility by means of reaction kinetics, electrolyte conductivity, diffusion co-efficient and viscosity. In the case of zinc-bromine batteries, the operating temperatures are between 20 and 50 °C and have little influences on overall energy efficiencies as shown in Figure 14. At low temperature, the electrolyte resistivity increases, resulting in lower voltage efficiencies, which are offset by the higher coulombic efficiencies attributed to slow bromine transport. At high temperature, the resistance decreases but with higher bromine transport., which partially compensating for each other [196, 200].

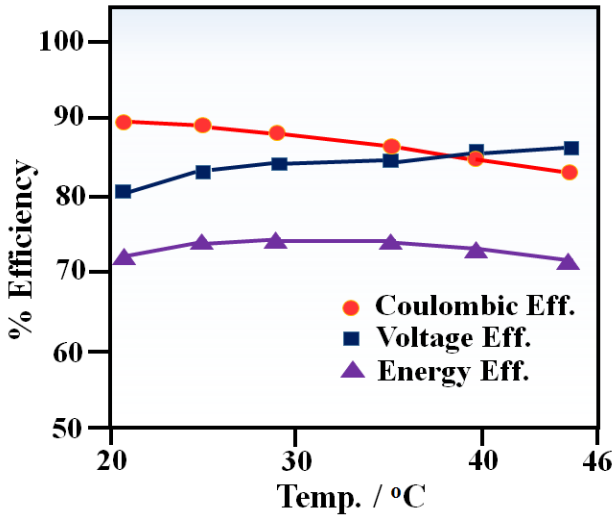

Figure 14. Influence of temperature on system efficiencies of a zinc-bromine hybrid flow batteries [200].

.

5.5. Hydrogen evolution

Hydrogen evolution tends to take place concurrently with zinc electrodeposition as a side reaction at the negative electrodes, which is considered as a major loss of current efficiencies at high current densities. Depending on the pHs of the solutions, the hydrogen overpotential can be as high as 1.0 V with suitable organic additives and substrate materials [248]. When metal substrate is used, the rates of hydrogen adsorption and evolutions tend to be higher in the conditions of high current density, low temperature and pH [248, 249]. In the absence of organic additives, zinc electrodeposition with over 90 % half-cell coulombic efficiencies are often obtained with carbon-based substrates at relatively high current densities (at 50 mA cm^{-2}) in several acid electrolytes [35, 86]. The mechanisms of hydrogen adsorptions and evolutions have been discussed in previous literatures [248, 250-253].

In the field of zinc electroplating, cationic surfactants are often used to suppress hydrogen evolutions [254-258], while preventing the growths of mossy and dendritic morphologies [254, 259-261]. In particular, cetyl trimethylammonium-based surfactants are commonly used and known to suppress hydrogen evolutions at low cost [258]. Other organic inhibitors for suppressing hydrogen evolution include tartaric acid, succinic acid and phosphoric acid, which also provide levelling performance for zinc electrodepositions [262]. However, some of these organic additives have large molecular weight or long hydrocarbon chain, the strong absorption and inhibiting effect often decrease the half-cell coulombic efficiencies [86] and slow down the charge-transfer processes [263]. Inorganic inhibitors often includes soluble salts or metal oxides of indium, bismuth, tin, gallium, thallium, bismuth and lead used in aqueous electrolytes [144, 264]. It should be noted that some of these elements are toxic or hazardous to the environments.

5.6. Zinc corrosion

Since zinc is an active materials, corrosion or self-dissolution of zinc leads to energy losses of battery systems. According to Pourbaix diagrams, no surface oxides are stable in acidic solutions, instead zinc dissolution and hydrogen evolution tend to take place simultaneously as mixed electrode reactions on the surfaces. In general, higher rates of dissolutions and hydrogen evolutions are observed at higher proton/acid concentrations. However, the rate of dissolutions might become lower at certain high acid concentrations (i.e. > 6 M) due to the lower availability of dissociated protons in the solutions [54]. In the pH range 1 to 4, this process is *via* cathodic control and the kinetics of the hydrogen evolution dictates the overall corrosion [265].

In alkaline solutions, zinc corrosion products formed are mainly zinc oxide and $ZnOH^+$ according to thermodynamic, which are not an effective protection barrier. In the pH range 4 to 11, the corrosion rates do not vary significantly attributed to the change in the cathodic reaction from hydrogen evolution to oxygen reduction. When the local pH is between 11 and 12, protective zinc oxides may be formed at certain negative electrode potentials, although the minimal corrosion may take place at lower pH in the alkaline solutions (i.e. pH 10 to 12) [265].

In general, the corrosion rates are highly influenced by the morphology and crystallographic planes, which are highly influenced by the electrolyte compositions [266]. Crystallographic and close packed planes tend to have higher binding energy of the surface atoms, resulting in better corrosion resistance. Other studies demonstrates that electrodeposits with finer grain size tend to have higher hardness and corrosion resistance [24, 25, 267, 268]. The uses of organic additives in both acidic and alkaline solutions often improve the electrodeposit morphologies and offer high current efficiency of > 90 % at < 40 mA cm^{-2}. The resulting electrodeposits also show improved corrosion resistance in corrosive chloride solutions than the electrodeposits obtained in the absence of additives [269].

Apart from improving zinc morphologies, some electrolyte additives also serve as corrosion inhibitors. Organic additives, particularly surfactants, often inhibit corrosion effectively by adsorption, and geometrically blocking of the zinc surfaces. On the other hand, inorganic additives, such as lead and indium, often form less chemically active metallic layers on the zinc surface. However, these inhibition effects are sometimes temporary over prolonged period of time (i.e. 10 h) as the adsorption of organic additives and the metallic layers may not be

lasting over times, especially under continued hydrogen evolutions [54]. Due to the strong adsorption and blocking of certain additives, there is no guarantee of high half-cell efficiencies suitable for zinc-based battery applications.

6. Applications of zinc-hybrid flow batteries

Due to the increased share of intermittent renewable energy sources, redox (or hybrid) flow batteries have become one of the most popular energy storage devices for grid-scale applications. Despite various flow battery chemistries, only all-vanadium, zinc-bromine, zinc-cerium, zinc-nickel and zinc-iron (zinc-ferricyanide) have been successfully scaled-up or commercialized from kW to MW scales. In addition to all-vanadium, the other systems are all based on zinc negative electrodes and exhibit higher operating voltages (≥ 1.58 V *vs.* 1.4 V of all-vanadium) (Figure 15.). The chemistries of these scaled-up or commercial systems have been introduced for more than a decade, their specifications and installation information have been summarized in Tables 2.

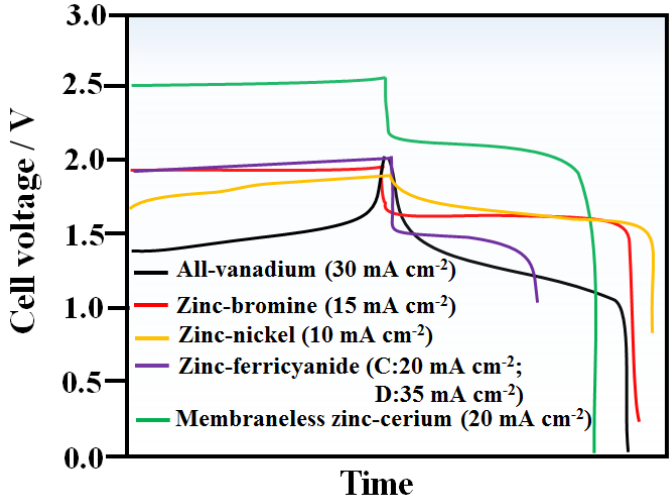

Figure 15. Cell voltage *vs.* time response during charge-discharge cycle for all-vanadium (30 mA cm^{-2} for 2 h) [66], zinc-bromine (15 mA cm^{-2} for 10 h) [196], zinc-nickel (10 mA cm-2 for *c.a.* 2 h [55, 115]), zinc-ferricyanide (charging at 20 mA cm^{-2} for *c.a.* 1.5 h; discharging at 35 mA cm^{-2}) [270] and the undivided zinc-cerium (20 mA cm^{-2} for 30 mins) [58, 59] hybrid flow batteries.

Among these zinc-based systems, zinc-bromine batteries have been the most studied systems and have been used in a number of applications, including load-levelling (up to MW), power quality control, coupling with renewable energy sources and electric vehicles (Table x, Figure 16). Other zinc-based flow batteries (i.e. zinc-nickel, zinc-cerium and zinc iron) have been demonstrated at smaller scale (kW) for load-leveling and energy storage for renewable energy sources. Load-levelling a strategy to store excess energy from a power plant during off-peak hours and release it when demand rises. Zinc-bromine hybrid flow batteries has been demonstrated for prolonged charging of up to 10 h [196], which is as competitive as commercial vanadium redox flow batteries.

Early grid-scale application of zinc-bromine batteries from 1 kW to 60 kW modules have been demonstrated through Moonlight project partly sponsored by Japanese government in the 1980s. These modules were later used in a 1 MW/4 MW h system in Fukuoka by Kyushu Electric Power Company (Japan), which consisted of twenty four 25 kW modules and has been the largest zinc-bromine system. In the 1980s, Exxon (United States)'s patent of zinc-bromine flow battery was transferred to Johnson Control Inc. (USA) and licensed to Studiengesellschaft für Energiespeicher and Antriebssysteme, S.E.A. (later known as Powercell, Austria), Toyota Motor (Japan), Meidensha (Japan) and Sherwood Industries (Australia). In Australia, several Exxon's systems at 3 – 20 kW have been installed in Australia for demonstration purpose. Meanwhile, research and development on zinc-bromine batteries have been carried out in Australia by Murdoch University (Parker and co-workers) and ZBB technologies

(Australia, recently as Ensync Energy System, United States). ZBB technologies expanded its business in the United States and acquired the assets of Johnson Controls, Inc. (United States) to manufacture zinc-bromine batteries [271]. In 2004, ZBB Technology was awarded a contract from California Energy Commission to demonstrate a 2 MW/ 2 MW h system for load-levelling applications [200].

In United States, Premium Power Corp. (United States, recently as Vionx Energy, United States) used the technology developed by Powercell (Austria. formerly S.E.A., Austria) but manufactured all-vanadium batteries nowadays. Since the 2000s, Redflow Ltd. (Australia) and Primus Inc. (United States) manufactured zinc-bromine flow batteries for household and load-levelling applications (up to 600 kW h). As claimed by Primus Inc., a membrane-less system was developed and ready for commercialization[272]. Zinc-cerium technology has been developed and scaled-up by Plurion Inc. (Scotland) and Applied Intellectual Capital (United States) up to kW scale until recent years. Since the 2010s, ViZn Energy Inc. (a former zinc-air battery company, Zinc Air Inc., United States) manufactures zinc-iron (zinc-ferricyanide) flow batteries for load-levelling applications from kW to MW scales [273].

Following the oil crisis in 1970s, Energy Development Associates (United States) has investigated the use of a 50 kWh zinc-chlorine flow batteries for electric vehicle applications. Since the Exxon project in the 1980s, S.E.A.(Austria) has tested a number of batteries ranging from 5 and 45 kW h in several electric vehicles accumulating more than 80,000 km [200, 274, 275]. This company has installed a 45 kW h, 216 V battery in a Volkswagen bus used for Austrian Postal Service in mountain areas. The battery weighted about 700 kg and allow maximum range of up to 220 km at 50 km h^{-1} (Figure 16c) [200]. In the 1990s, electric vehicles with zinc-bromine batteries have also been tested by University of California (a 35 kW h system) and demonstrated by Toyota Motor (Japan) as model EV-3036 (7 kW h, 106 V) [200]. Fiat Automobilesb (Italy) has also installed a 18 kW h zinc-bromine battery (72 V, 250 A h) in Fiat Panda city car. Hotzenblitz GmbH (Germany) has also designed an electric vehicle with a 15 kW h / 114 V zinc-bromine battery. Despite relatively high life-time, lack of adequate peak power of zinc-bromine flow battery has been the main obstacle for electric vehicle applications[275]
.

	Zinc-bromine	**Zinc-cerium**	**Zinc-nickel**	**Zinc-iron (Zinc-ferricyanide)**
Cell open-circuit voltage/ V	1.8	2.4	1.73	1.53
Energy density/ W h L^{-1}	Up to 60	12–20	Up to 50	-
Cycle round-trip DC energy efficiency/ %	65–75	63	>85	65-75
Cycle life (cycles)	>2 000	NG	>500	>5000
Operating Temp. /°C	50	60	30-50	45
Total system cost/ USD$ kW^{-1}	1044	750	-	>300

Cost attribution of storage module / %	80	50	-	-
Typical size range / MW h	0.01–5	NG	0.1	0.04-2
Unit design life time/years	5–10	15	>5	20
Stage of development	Demonstration /Commercial units	Demonstration	Demonstration	Demonstration/ Commercial units
Major companies involved	ZBB Energy (recently as Ensync Energy System), Premium Power (recently as Vionx Energy) , Kyushu Electric Power, Meidensha, Primus Power and Redflow	Plurion	Urban Electric Power	ViZn Energy System
Number of installations	>10	2	1	>5
Largest installation	1 MW in Kyushu, by Kyushu Electric Power	2 kW – 1 MW testing facility in Glenrothes, Scotland by Plurion	100kW in New York, US by Urban Electric Power	1000 kW in ComEd Bronzeville, US by ViZn Energy System

Table x. Specifications and installation information of commercial zinc-based hybrid flow batteries.

System	Company	Customer	Basic specification	Application	Installation date
Zinc-bromine	ZBB Energy	Detroit Edison, United States	400 kW h	Load levelling	Jun 2001
		United Energy, Melbourne, Australia	200 kW h	Demonstration for network storage applications	Nov 2001
		Nunawading Electrical Distribution Substation in	400 kW h	Load levelling	2001

		Box Hill, Australia			
		Australian Inland Energy, Australia	500 kW h	Solar energy	Jun 2002
		Power Light, United States	2 × 50 kW h	Solar energy	Nov 2003
		Pacific Gas and Electric Co., United States	2 MW h	Peak power capacity	Oct 2005
		Dundalk Institute of Technology, Ireland	125 kW / 500 kW h	Wind energy	Dec 2008
		Illinois Institute of Technology, United States	500 kW h	Microgrid	Sept 2014
		Fort Sill,Oklahoma, United States	500 kW h	Microgrid	2013
		Pualani Manor, United States		Solar energy	2013
	Kyushu Electric Power & Meidensha	Imajuku substation in Kyushu Electric Power, Japan	1 MW/ 4 MW h	Electric-utility applications	1990
	Redflow	University of Queenland, Australia	12 × 120 kW h	Solar energy	Apr 2011
	Department of Energy,US	Albuquerque, New Mexico, United States	2.8 MW h	Solar energy	2011
	Vionx Energy (previously Premium Power)	Massachusetts, United States	0.5 MW / 3 MW h	Peak power capacity	Nov 2016
Zinc-cerium	Plurion	Glenrothes, Scotland	2 kW – 1 MW	Testing facility	2007
Zinc-nickel	Urban Electric Power	New York, United States	100 kW	Peak power capacity	Jun 2013

Zinc-iron	ViZn Energy System	Flathead Electric Cooperative, United States	80 kW/ 160 kWh	Utilities and power	Mar 2014
		BlueSky Energy, Austria	64 kW	Solar energy and Microgrid	Nov 2013
		Ontario, Canada	2 MW/ 6 MW h	Frequency regulation Ancillary services	Aug 2015
		Randolph-Macon College, US	48 kW	Solar energy	Apr 2015
		ComEd Bronzeville, United States	1000 kW	Solar energy	Mar 2016
		Idaho National Laboratory, United States	128 kW	Microgrid research	Jan 2016

Table x. Existing installations and applications of zinc-based hybrid flow batteries.

(a)

(b)

(c)

Figure 16. Installations of zinc-bromine hybrid flow batteries: (a) with solar energy at Marine Corps Air Station (MCAS) in Miramar, California by Primus Power Corp.; (b) with solar energy sites at New Zealand by Redflow Ltd.; (c) a Volkswagen bus used for Austrian Postal Service equipped with a 45 kWh/216 V zinc-bromide redox flow batteries by S.E.A. [276]

References

1. P. Leung, X. Li, C. Ponce de Leon, L. Berlouis, C.T.J. Low, F.C. Walsh, 'Progress in redox flow batteries, remaining challenges and their applications in energy storage', *RSC Adv*, **2** (2012) 10125-10156.
2. C. Ponce de Leon, A. Frias-Ferrer, J. Gonzalez-Garcia, D.A. Szanto, F.C. Walsh, 'Redox flow cells for energy conversion', *J. Power Sources*, **160** (2006) 716-732.
3. R.F. Service, 'Tank for the Batteries', *Science*, **344,** (2014) 352-354.
4. G. Kear, A.A. Shah, F.C. Walsh, 'Development of the all-vanadium redox flow battery for energy storage: a review of technological, financial and policy aspects', *Int. J. Energy Res.*, **36** (2012) 1105-1120.
5. Office of Electricity Delivery & Energy Reliability, ' Grid Energy Storage - December 2013'. U.S. Department of Energy, https://energy.gov/oe/downloads/grid-energy-storage-december-2013 accessed on 3 Aug 2017.
6. J. Winsberg, T. Hagemann, T. Janoschka, M.D. Hager, U.S. Schubert, 'Redox-Flow Batteries: From Metals to Organic Redox-Active Materials', *Angew. Chem. Int. Ed.*, **56** (2016) 686-711.
7. M. Park, J. Ryu, W. Wang, J. Cho, 'Material design and engineering of next-generation flow battery technologies', *Nature Reviews*, article-in-press.
8. P. Leung, A.A. Shah, L. Sanz, C. Flox, J.R. Morante, Q. Xu, M.R. Mohamed, C.P.d. Leon, F.C. Walsh, 'Recent developments in organic redox flow batteries: A critical review', *J. Power Sources*, **360** (2017) 243–283.
9. Y. Xu, Y. Wen, J. Cheng, G. Gao, Y. Yang, 'Study on a single flow acid Cd-chloranil battery', *Electrochemistry Communications*, **11** (2009) 1422-1424.
10. J. Winsberg, T. Hagemann, T. Janoschka, M.D. Hager, U.S. Schubert, 'Redox-Flow Batteries: From Metals to Organic Redox-Active Materials', *Angew. Chem. Int. Ed.*, **56** (2017) 686-711 http://onlinelibrary.wiley.com/doi/10.1002/anie.201604925/full.
11. London Metal Exchange, https://www.lme.com/Metals/Non-ferrous/Zinc#tabIndex=0 accessed on 3 Aug 2017.
12. M. Fleischmanm, L.R. Hill, G. Sundholm, ' *J. Electroanal. Chem.*, **157** (1983) 359-368.
13. D.W. McComsey, 'Handbook of Batteries', 3rd Ed. McGraw Hill, **8** (2002) 184-228
14. K. Kordesch, J.Daniel-Ivad, 'Handbook of Batteries', McGraw-Hill, New York, **Chapter 36** (2002) 1168-1185
15. X.G. Zhang, 'Corrosion and Electrochemistry of Zinc', 1 Ed. Springer, **Chapter 1** (1996) 1-16
16. D. Crotty, 'Zinc Alloy Plating for the Automotive Industry', *J. Met. Finish.*, **94** (1996) 54-58.
17. E. Budman, R.R. Sizelove, 'Zinc Alloy Plating', *J. Met. Finish.*, **99** (2001) 334-339.
18. H.H. Geduld, 'Zincate or Alkaline Noncyanide Zinc Plating', *ASM International, Metals Park, Ohio*, (1988) 90-106.
19. G. Trejo, Y. Meas, P. Ozil, E. Chainet, 'Nucleation and Growth of Zinc from Chloride Concentrated Solutions', *J. Electrochem. Soc.*, **145** (1998) 4090-4097.
20. P. Díaz-Arista, Y. Meas, R. Ortega, G. Trejo, 'Electrochemical and AFM study of Zn electrodeposition in the presence of benzylideneacetone in a chloride-based acidic bath', *J. Appl. Electrochem.*, **35** (2005) 217-227.
21. M. Schlesinger, M. Paunovic, 'Modern Electroplating', 4 Ed. John Wiley & Sons Inc., (2000)
22. F.A. Lowenheim, 'Electroplating', Technical Reference Publications, (1995)
23. K.M.S. Youssef, C.C. Koch, P.S. Fedkiw, 'Improved corrosion behavior of nanocrystalline zinc produced by pulse-current electrodeposition', *Corros. Sci.*, **46** (2004) 51-64.
24. M.S. Youssef, C.C. Koch, P.S. Fedkiw, 'Influence of Additives and Pulse Electrodeposition Parameters on Production of Nanocrystalline Zinc from Zinc Chloride Electrolytes', *J. Electrochem. Soc.*, **151** (2004) C103-C111.
25. A. Gomes, M.I. da Silva Pereira, 'Pulsed electrodeposition of Zn in the presence of surfactants ', *Electrochim. Acta*, **51** (2006) 1342-1350.
26. A.E. Saba, A.E. Elsherief, 'Continuous electrowinning of zinc', *Hydrometallurgy*, **54** (2000) 91-106.
27. J. Yu, Y. Chen, H. Yang, Q. Huang, 'The Influences of Organic Additives on Zinc Electrocrystallization from KCl Solutions', *J. Electrochem. Soc.*, **146** (1999) 1789-1793.
28. A. Gomes, M.I.d.S. Pereira, 'Zn electrodeposition in the presence of surfactants: Part I. Voltammetric and structural studies', *Electrochim. Acta*, **52** (2006) 863-871.
29. A.M. Alfantazi, D.B. Dreisinger, 'An investigation on the effects of orthophenylene diamine and sodium lignin sulfonate on zinc electrowinning from industrial electrolyte', *Hydrometallurgy*, **69** (2003) 99-107.

30. A. Gomes, A.S. Viana, M.I.d.S. Pereira, 'Potentiostatic and AFM morphological studies of Zn electrodeposition in the presence of surfactants', *J. Electrochem. Soc.*, **154** (2007) D452-D461.
31. K. Gong, Q.R. Fang, S. Gu, S.F.Y. Li, Y.S. Yan, 'Nonaqueous Redox-Flow Batteries: Organic Solvents, Supporting Electrolytes, and Redox Pairs', *Energy Environ. Sci.*, **8** (2015) 3515-3530.
32. J.W. Gallaway, C.K. Erdonmez, Z. Zhong, M. Croft, L.A. Sviridov, T.Z. Sholklapper, D.E. Turney, S. Banerjee, D.A. Steingart, 'Real-time materials evolution visualized within intact cycling alkaline batteries ', *J. Mater. Chem. A*, **2** (2014) 2757-2764.
33. R. Patrice, B. Gerand, J.B. Leriche, L. Seguin, E. Wang, R. Moses, K. Brandt, J.M. Tarascon, 'Understanding the second electron discharge plateau in MnO2-based alkalinecells', *J. Electrochem. Power Sources*, **148** (2001) A448-A455.
34. M. Chamoun, B.J. Hertzberg, T. Gupta, D. Davies, S. Bhadra, B.V. Tassell, C. Erdonmez, D.A. Steingart, 'Hyper-dendritic nanoporous zinc foam anodes', *NPG Asia Materials*, **7** (2015) https://www.nature.com/am/journal/v7/n4/full/am201532a.html (Published online 24 April 2015).
35. J. Pan, Y. Wen, J. Cheng, J. Pan, Z. Bai, Y. Yang, 'Zinc deposition and dissolution in sulfuric acid onto a graphite-resin composite electrode as the negative electrode reactions in acidic zinc-based redox flow batteries', *J. Appl. Electrochem.*, **43** (2013) 541-551.
36. X. Li, D. Pletcher, C. Ponce de Léon, F.C. Walsh, R.G.A. Wills, 'Redox flow batteries for energy storage using zinc electrodes', in 'Advances in batteries for large- and medium-scale energy storage: Applications in power systems and electric vehicles', (eds. C. Menictas, M. Skyllas-Kazacos, T.M. Lim);' *Woodhead*, (2015) 293-315.
37. M. Skyllas-Kazacos, M.H. Chakrabarti, S.A. Hajimolana, F.S. Mjalli, M. Saleem, 'Progress in Flow Battery Research and Development', *J. Electrochem. Soc.*, **158** (2011) R55-R79.
38. A.Z. Weber, M.M. Mench, J.P. Meyers, P.N. Ross, J.T. Gostick, Q. Liu, 'Redox flow batteries: a review', *J. Appl. Electrochem*, **41** (2011) 1137-1164.
39. J. Noack, N. Roznyatovskaya, T. Herr, P. Fischer, 'The Chemistry of Redox-Flow Batteries', *Angew. Chem. Int. Ed.*, **54** (2015) 9776-9809.
40. S.H. Shin, S.H. Yun, S.H. Moon, 'A review of current developments in non-aqueous redox flow batteries: characterization of their membranes for design perspectives', *RSC Adv.*, **3** (2013) 9095-9116.
41. F. Pan, Q. Wang, 'Redox Species of Redox Flow Batteries: A Review', *Molecules*, **20** (2015) 20499-20517.
42. Q. Huang, Q. Wang, 'New-Generation, High-Energy-Density Redox Flow Batteries', *ChemPlusChem*, **80** (2015) 312-322.
43. Q. Xu, T.S. Zhao, 'Fundamental models for flow batteries', *Prog. Energy Combust. Sci.*, **49** (2015) 40-58.
44. R.M. Darling, K.G. Gallagher, J.A. Kowalski, S. Ha, F.R. Brushett, 'Pathways to low-cost electrochemical energy storage: a comparison of aqueous and nonaqueous flow batteries', *Energy Environ. Sci.*, **7** (2014) 3459-3477.
45. C. Choi, S. Kim, R. Kim, Y. Choi, S. Kim, H.Y. Jung, J.H. Yang, H.T. Kim, 'A review of vanadium electrolytes for vanadium redox flow batteries', *Renewable and Sustainable Energy Reviews*, **69** (2017) 263-274.
46. A. Parasuraman, T.M. Lim, C. Menictas, M. Skyllas-Kazacos, 'Review of material research and development for vanadium redox flow battery applications', *Electrochim. Acta*, **101** (2013) 27-40.
47. K.J. Kim, M.S. Park, Y.J. Kim, J.H. Kim, S.X. Dou, M. Skyllas-Kazacos, 'A technology review of electrodes and reaction mechanisms in vanadium redox flow batteries', *J. Mater. Chem. A*, **3** (2015) 16913-16933.
48. Y. Zhao, Y. Ding, Y. Li, L. Peng, H.R. Byon, J.B. Goodenough, G. Yu, 'A chemistry and material perspective on lithium redox flow batteries towards high-density electrical energy storage', *Chem. Sov. Rev.*, **44** (2015) 7968-7996.
49. 'Zinc-Periodic Table'. Royal Society of Chemistry, http://www.rsc.org/periodic-table/element/30/zinc accessed on 3 Aug 2017.
50. J.B. Calvert, 'Zinc and Cadmium, University of Denver', http://mysite.du.edu/~jcalvert/phys/zinc.htm.
51. B. Berverskog, I. Puigdomenech, 'Revised Poubaix diagrams for zinc at 25-300 ºC', *Corros. Sci.*, **39** (1997) 107-114.
52. 'The Nernst Equation and Pourbaix diagram, '. TLP Library, DoITPoMS, University of Cambridge, https://www.doitpoms.ac.uk/tlplib/pourbaix/index.php accessed on 3 Aug 2017.
53. T.K.A. Hoang, T.N.L. Doan, K.E.K. Sun, P. Sun, 'Corrosion chemistry and protection of zinc & zinc alloys by polymer-containing materials for potential use in rechargeable aqueous batteries', *RSC Adv.*, **5** (2015) 41677-41691.

54. P. Leung, C. Ponce-de-León, F. Recio, P. Herrasti, F. Walsh, 'Corrosion of the zinc negative electrode of zinc-cerium hybrid redox flow batteries in methanesulfonic acid', *J. Appl. Electrochem.,* **44** (2014) 1025-1035.
55. L. Zhang, J. Cheng, Y.S. Yang, Y.H. Wen, X.D. Wang, G.P. Cao, 'Study of zinc electrodes for single flow zinc/nickel battery application', *J. Power Sources,* **179** (2008) 381-387.
56. S. Banerjee, Y. Ito, M. Klein, M.E. Nyce, D. Steingart, R. Plivelich et al., 'Nickel-zinc flow battery', US patent 20130113431 A1, (2013).
57. P.K. Leung, Q. Xu, T.S. Zhao, 'High-potential zinc-lead dioxide rechargeable cells', *Electrochim. Acta.,* **79** (2012) 117-125.
58. P.K. Leung, T. Martin, A.A. Shah, M.A. Anderson, J. Palma, 'Membrane-less organic-inorganic aqueous flow batteries with improved cell potential', *Chem Comm.,* (2017) article in press.
59. P.K. Leung, T. Martin, A.A. Shah, M.R. Mohamed, M.A. Anderson, J. Palma, 'Membrane-less hybrid flow battery based on low-cost elements', *J. Power Sources,* **341** (2017) 36-45.
60. P.K. Leung, C. Ponce de Leon, F.C. Walsh, 'An undivided zinc-cerium redox flow battery operating at room temperature (295 K)', *Electrochemistry Communications,* **13** (2011) 770-773.
61. A. Hazza, D. Pletcher, R. Wills, 'A novel flow battery: A lead acid battery based on an electrolyte with soluble lead(II) Part I: Preliminary studies', *Phys. Chem. Chem. Phys.,* **6** (2004) 1773-1778.
62. P.K. Leung, X. Li, C. Ponce de León, L. Berlouis, C.T.J. Low, F.C. Walsh, 'Progress in redox flow batteries, remaining challenges and their applications in energy storage', *RSC Advances,* **2** (2012) 10125-10156.
63. C. Ponce de León, A. Frías-Ferrer, J. González-García, D.A. Szánto, F.C. Walsh, 'Redox flow cells for energy conversion', *J. Power Sources,* **160** (2006) 716-732.
64. H. Liu, Q. Xu, C. Yan, Y. Qiao, 'Corrosion behavior of a positive graphite electrode in vanadium redox flow battery', *Electrochim. Acta,* **56** (2011) 8783-8790.
65. L. Wei, T.S. Zhao, Q.Xu, X.L. Zhou, Z.H. Zhang, ' In-situ investigation of hydrogen evolution behaviour in vanadium redox flow batteries', *Applied Energy,* **190** (2017) 1112-1118.
66. M. Kazacos, M. Skyllas-Kazacos, 'Performance Characteristics of Carbon Plastic Electrodes in the All-Vanadium Redox Cell', *J. Electrochem. Soc.,* **136-9** (1989) 2759-2760.
67. S. Zhong, M. Kazacos, R.P. Burford, M. Skyllas-Kazacos, 'Fabrication and activation studies of conducting plastic composite electrodes for redox cells', *J. Power Sources,* **36** (1991) 29-43.
68. P. Qian, H.M. Zhang, J. Chen, Y.H. Wen, Q.T. Luo, Z. Liu, D.J. You, B.L. Yi, 'A novel electrode-bipolar plate assembly for vanadium redox flow battery applications', *J. Power Sources,* **175** (2008) 613-620.
69. M.S. Yazici, D. Krassowski, J. Prakash, 'Flexible graphite as battery anode and current collector', *J. Power Sources,* **141** (2005) 171-176.
70. M.S. Pereira, L.L. Barbosa, C.A.C. Souza, A.C.M.D. Moraes, I.A. Carlos, 'The influence of sorbitol on zinc film deposition, zinc dissolution process and morphology of deposits obtained from alkaline bath', *J. Appl. Electrochem.,* **36** (2006) 727-732.
71. J.X. Yu, H.X. Yang, X.P. Ai, Y.Y. Chen, 'Effects of Anions on the Zinc Electrodeposition onto Glassy-Carbon Electrode', *Russian J. Electrochem.,* **38** (2002) 321-325.
72. J. Heinze, A. Rasche, M. Pagels, B. Geschke, 'On the origin of the so-called nucleation loop during electropolymerization of conducting polymers', *J. Phys. Chem. B,* **111** (2007) 989-997.
73. E. Budevski, G. Staikov, W.J. Lorenz, 'Electrocrystallization: Nucleation and growth phenomen', *Electrochim. Acta,* **45** (2000) 2559-2574.
74. F.C. Walsh, M.E. Harron, 'Electrocrystallization and electrochemical control of crystal growth: fundamental considerations and electrodeposition of metals', *J. Phys. D: Appl. Phys.* , **24** (1991) 217 - 225.
75. I.N. Stranski, 'Stoechiom. Verwandtschaftsl', *Z. Phys. Chem.* , **136** (1928) 297.
76. I.N. Stranski, R. Kaischew, ' *Z. Phys. Chem.,* **B 24** (1934) 100.
77. I.N. Stranski, R. Kaischew, ' *Z. Phys. Chem.* , **B 26** (1934) 312.
78. R. Kaischew, I.N. Stranski, ' *Z. Phys. Chem.,* **B 26** (1934) 114.
79. R. Kaischew, I.N. Stranski, ' *Z. Phys. Chem.,* **B 26** (1934) 317.
80. R. Kaischew, I.N. Stranski, ' *Z. Phys. Chem.,* **170** (1934) 295.
81. R. Becker, W. Döring, 'Kinetische Behandlung der Keimbildung in übersättigten Dämpfen', *Ann. Phys.,* **24** (1935) 719.
82. P.A. Adcock, A. Quillinan, B. Clark, O.M.G. Newman, S.B. Adeloju, 'Measurement of Polarization Parameters Impacting on Electrodeposit Morphology. II: Conventional Zinc Electrowinning Solutions', *J. Appl. Electrochem.,* **34** (2004) 771-780.
83. K. Raeissi, A. Saatchi, M.A. Golozar, 'Effect of nucleation mode on the morphology and texture of electrodeposited zinc', *J. Appl. Electrochem.,* **33** (2003) 635-642.

84. R.Y. Wang, D.W. Kirk, G.X. Zhang, 'Effects of Deposition Conditions on the Morphology of Zinc Deposits from Alkaline Zincate Solutions', *J. Electrochem. Soc.,* **153** (2006) C357-C364.
85. N. Soroura, W. Zhanga, E. Ghalia, G. Houlachi, 'A review of organic additives in zinc electrodeposition process (performance and evaluation)', *Hydrometallurgy,* **171** (2017) 320-332 http://www.sciencedirect.com/science/article/pii/S0304386X17300373
86. P. Leung, C. Ponce de Leon, C.T.J. Low, F.C. Walsh, 'Zinc deposition and dissolution in methanesulfonic acid onto a carbon composit electrode as the negative electrode reactions in a hybrid redox flow battery', *Electrochim. Acta,* **18** (2011) 6536-6546.
87. R.A. Putt 'Assessment of technical and economic feasibility of zinc/bromine batteries for utility load leveling. Final report'; Researchgate: (1979) https://www.researchgate.net/publication/253499892_Assessment_of_technical_and_economic_feasibility_of_zincbromine_batteries_for_utility_load_leveling.
88. N. Clark, P. Eidler, P. Lex 'Development of Zinc/Bromine Batteries for Load-Levelling Applications: Phase 2 Final Report'; SAND99-2691; Sandia: (1999) http://prod.sandia.gov/techlib/access-control.cgi/1999/992691.pdf.
89. P. Leung, C. Ponce de Leon, C.T.J. Low, F.C. Walsh, 'Ce(III)/Ce(IV) in methanesulfonic acid as the positive half cell of a redox flow battery', *Electrochim. Acta,* **56** (2011) 2145-2153.
90. S.C. Yang, 'An approximate model for estimating the faradaic efficiency loss in zinc/bromine batteries caused by cell self-discharge', *J. Power Sources,* **50** (1994) 343-360.
91. J.E. Oxley 'The Improvement of Zinc Electrodes for Electrochemical Cells'; NASA, ASA Contractor Report: (1966) http://ntrs.nasa.gov/archive/nasa/casi.ntrs.nasa.gov/19660006505_1966006505.pdf.
92. K.I. Popov, M.G. Pavlović, M.D. Spasojević, V.M. Nakić, 'The Critical Overpotential for Zinc Dendrite Formation', *J. Appl. Electrochem.,* **9** (1979) 533-536.
93. V. Konschuter, ' *J. Trans. Electrochem. Soc.,* **45** (1924) 229.
94. J. Torrent-Burgues, E. Guaus, F. Sanz, 'Initial stages of tin electrodeposition from sulfate baths in the presence of gluconate', *J. Appl. Electrochem.,* **32** (2002) 225-230.
95. A.M. Volmer, Z. Weber, 'Nuclei formation in supersaturated states', *J. Phys. Chem.,* **119** (1926) 277-301.
96. M.C. Li, S.Z. Luo, Y.H. Qian, W.Q. Zhang, L.L. Jiang, J.I. Shen, 'Effective of Additives on Electrodeposition of Nanocrystalline Zinc from Acidic Sulfate Solution', *J. Electrochem. Soc.,* **154** (2007) D567-D571.
97. M. Mouagnga, L. Ricq, J. Douglade, P. Berc, ' *J. Appl. Electrochem.,* **37** (2007) 283-289.
98. D.J. MacKinnon, J.M. Brannen, 'Evaluation of organic additives as levelling agents for zinc electrowinning from chloride electrolytes', *J. Appl. Electrochem.,* **12** (1982) 21-31.
99. E. Michailova, M. Peykova, D. Stoychev, A. Milchev, 'On the role of surface active agents in the nucleation step of metal electrodeposition on a foreign substrate', *J. Electroanal. Chem.,* **366** (1994) 195-202.
100. D.A. Vermilyea, 'Electrodeposition onto Metal Whiskers', *J. Chem. Phys.,* **27** (1957) 814.
101. P.B. Price, D.A. Vermilyea, M.B. Webb, 'On the growth and properties of electrolytic whiskers', *J. Acta Metallurgica,* **6** (1958) 524-531.
102. H. Fischer, 'Wirkungen der inhibitoren bei der elektrokristallisation: Übersicht über den gegenwärtigen stand der forschung', *Electrochim. Acta,* **2** (1960) 50-91.
103. G. Trejo, H. Ruiz, R. Ortega Borges, Y. Meas, 'Influence of polyethoxylated additives on zinc electrodeposition from acidic solutions', *J. Appl. Electrochem.,* **31** (2001) 685-692.
104. L.M. Mureşan, S.C. Varvara, 'Levelling and Brightening Mechanisms in Metal Electrodeposition, and Nunez Magdalena, Metal Electrodeposition', Nova Science Publishers, **59** (1955) 756-766
105. D.G. Foulke, O. Kardos, 'Current distribution in microprofiles', *Proc. Am. Electroplaters Soc.,* **43** (1956) 172-181.
106. H.Z. Leidheiser, ' *J. Elekrochem.,* **21** (1991) 565-574.
107. J.L. Fang, 'Theory and Application of Electroplating Additives', (2006) 365-373
108. 'Practical Plating Additives 實用電鍍添加劑 (Chinese book)', (2007)
109. D.E. Turney, J.W. Gallaway, G.G. Yadav, R. Ramirez, M. Nyce, S. Banerjee, Y.K. Chen-Wiegart, J. Wang, M.J. D'Ambrose, S. Kolhekar, J. Huang, X. Wei, 'Rechargeable zinc alkaline anodes for long-cycle energy storage', *Chem. Mater.,* **29** (2017) 4819-4832.
110. Y. Ito, M. Nyce, R. Plivelich, M. Klein, D. Steingart, S. Banerjee, 'Zinc morphology in zinc-nickel flow assisted batteries and impact on performance ', *J. Power Sources,* **196** (2011) 2340-2345.
111. T. Michaelowski, 'Russian Patent, Group XI, No. 5100, (1901).
112. D. Coates, A. Charkey, 'Handbook of Batteries, Chapter 31 Nickel-Zinc Batteries', 3rd Ed. McGraw Hill, (2002)

113. Y. Ito, X. Wei, D. Desai, D. Steingart, S. Banerjee, 'An indicator of zinc morphology transition in flowing alkaline electrolyte', *J. Power Sources*, **211** (2012) 119-128.
114. G. Bronoel, 'Development of Ni-Zn cells', *J. Power Sources*, **34** (1991) 243-255.
115. J. Cheng, L. Zhang, Y.S. Yang, Y.H. Wen, G.P. Cao, X.D. Wang, 'Preliminary Study of single flow zinc-nickel battery', *Electrochem. Commun.*, **9** (2007) 2639-2642.
116. Y. Cheng, X. Xi, D. Li, X. Li, Q. Lai, H. Zhang, 'Performance and potential problems of high power density zinc-nickel single flow batteries', *RSC Advances*, **5** (2015) 1772-1776.
117. Y. Cheng, Q. Lai, X. Li, X. Xi, Q. Zheng, C. Ding, H. Zhang, 'Zinc-nickel single flow batteries with improved cycling stability by eliminating zinc accumulation on the negative electrode', *Electrochim. Acta*, **145** (2014) 109-115.
118. Y. Cheng, H. Zhang, Q. Lai, X. Li, D. Shi, L. Zhang, 'A high power density single flow zinc-nickel battery with three-dimensional porous negative electrode', *J. Power Sources*, **241** (2013) 196-202.
119. D.E. Turney, M. Shmukler, K. Galloway, M. Klein, Banerjee, 'Development and testing of an economic grid-scale flow-assisted zinc/nickel-hydroxide alkaline battery', *J. Power Sources*, **264** (2014) 49-58.
120. N.J. Magnani, R.P. Clark, J.W. Braithwaite, D.M. Bush, P.C. Butler, J.M. Freese, K.R. Grothaus, K.D. Murphy, P.E. Shoemaker 'Exploratory Battery Technology Development and Testing Report for 1985'; Report No. SAND86- 1266 UC-94cb; Sandia National Laboratories: (1987) http://www.sandia.gov/ess/publications/SAND1986-1266.pdf.
121. M. Yang, H. Wu, J.R. Selman, 'A cycling performance model for the zinc/ferricyanide battery', *J. Chem Ind. & Eng. (China)*, **4** (1989) 93-114.
122. Y. Wen, T. Wang, J. Cheng, J. Pan, G. Cao, Y. Yang, 'Lead ion and tetrabutylammonium bromide as inhibitors of the growth of spongy zinc in single flow zinc/nickel batteries', *Electrochim. Acta*, **59** (2012) 64-68.
123. T.K. Hoang, M. Acton, H.T. Chen, Y. Huang, T.N.L. Doan, P. Chen, 'Sustainable gel electrolyte containing Pb 2+ as corrosion inhibitor and dendrite suppressor for the zinc anode in the rechargeable hybrid aqueous battery', *Materials Today Energy*, **4** (2017) 34-40.
124. C. Iwakura, H. Murakami, S. Nohara, N. Furukawa, H. Inoue, 'Charge–discharge characteristics of nickel/zinc battery with polymer hydrogel electrolyte', *J. Power Sources*, **152** (2005) 291-294.
125. S. Satoshi, O. Tsukasa, I. Yutaka, Y. Takao, 'Nickel-zinc alkaline storage battery', US Pat. 3976502, (1976).
126. S. Higashi, S.W. Lee, J.S. Lee, K. Takechi, Y. Cui, 'Avoiding short circuits from zinc metal dendrites in anode by backside-plating configuration', *Nat. Commun. 7*, Article number: 11801 https://www.nature.com/articles/ncomms11801.
127. S. Achiwa, ' *Shiga-Kenritsu Tanki Darguku Grakujutsu Zasshi (Japan)*, **16** (1975) 7.
128. E. Villarreal-Dominguez, 'Lead dioxide-zinc rechargeable type cell and battery and electrolyte therefore', US Pat. 3964927, (1976).
129. J.E. Stauffer, 'Lead zinc battery', EP 1555710, 20/07/2005, (2005).
130. M.S.E. Abdo, T.Z. Fahidy, 'Charge-discharge characteristics of a lead oxide-zinc secondary battery system', *J. Appl. Electrochem.*, **12** (1982) 225-230.
131. J. Pan, Y. Wen, J. Cheng, J. Pan, S. Bai, Y. Yang, 'Evaluation of substrates for zinc negative electrode in acid PbO2-Zn single flow batteries', *Chin. J. Chem. Eng.*, **24** (2016) 529-534.
132. J.Q. Pan, Y.Z. Sun, J. Cheng, Y.H. Wen, Y.S. Yang, P.Y. Wan, 'Study on a new single flow acid Cu-PbO_2 battery', *Electrochem. Commun.*, **10** (2008) 1226-1229.
133. J. Pan, M. Yang, X. Jia, Y. Sun, 'The principle and Electrochemical Performance of a Single Flow Cd-PbO2 Battery', *J. Electrochem. Soc.*, **100** (2013) A1146-A1152.
134. R.d. Surville, M. Josefowicz, L.T. Yu, J. Perichon, R. Buvet, 'Electrochemical chains using protolytic organic semiconductors ', *Electrochim. Acta*, **13** (1968) 1451-1458.
135. P. Novak, K. Muller, K.S.V. Santhanam, O. Haas, 'Electrochemically Active Polymers for Rechargeable Batteries', *Chem. Rev.*, **97** (1997) 207-281.
136. S.Q. Li, G.L. Zhang, G.L. Jing, J.Q. Kan, 'Aqueous zinc–polyaniline secondary battery', *J. Synthetic Metals*, **158** (2008) 242-245.
137. M. Sima, T. Visan, M. Buda, 'A comparative study of zinc—polyaniline electrochemical cells having sulfate and chloride electrolytes ', *J. Power Sources*, **56** (1995) 133-l36.
138. Y. Zhao, S.Si, C. Liao, 'A single flow zinc/polyaniline suspension rechargeable battery', *J. Power Sources*, **241** (2013) 449-453.
139. L.W. Hruska, R.F. Savinell, 'Investigation of Factors Affecting Performance of the Iron-Redox Battery', *J. Electrochem. Soc.*, **128** (1981) 18-25.

140. R. Amirante, E. Cassone, E. Distaso, P. Tamburrano, 'Overview on recent developments in energy storage: mechanical, electrochemical and hydrogen technologies', *Energy Conversion and Management*, **132** (2017) 372-387.
141. S. Selverston, R. Savinell, J. Wainright, 'Zinc-Iron Flow Batteries with Common Electrolyte', *J. Electrochem. Soc.*, **164** (2017) A1069-A1075.
142. Z. Xie, Q. Su, A. Shi, B. Yang, B. Liu, J. Chen, X. Zhou, D. Cai, L. Yang, 'High performance of zinc-ferrum redox flow battery with Ac-/HAc buffer solution', *J. Energy Chem.*, **25** (2016) 495-499.
143. K. Gong, X. Ma, K.M. Conforti, K.J. Kuttler, J.B. Grunewald, K.L. Yeager, M.Z. Bazant, S. Gu, Y. Yan, 'A zinc-iron redox-flow battery under $100 per kW h of system capital cost', *Energy & Environmental Science*, **8** (2015) 2941-2945.
144. R.L. Clarke, B.J. Dougherty, S. Harrison, P.J. Millington, S. Mohanta, 'Cerium Batteries', US 2004/ 0202925 A1, (2004).
145. R.L. Clarke, B.J. Dougherty, S. Harrison, J.P. Millington, S. Mohanta, 'Battery with bifunctional electrolyte', US 2006/0063065 A1, (2005).
146. B. Fang, S. Iwasa, Y. Wei, T. Arai, M. Kumagai, 'A study of the Ce (III)/Ce (IV) redox couple for redox flow battery', *Electrochim. Acta*, **47** (2002) 3971-3976.
147. P. Leung, C. Ponce de Leon, C.T.J. Low, A.A. Shah, F.C. Walsh, 'Characterization of a zinc-cerium flow battery', *J. Power Sources*, **196** (2011) 5174-5186.
148. P.K. Leung, C. Ponce de León, F.C. Walsh, 'An undivided zinc-cerium redox flow battery operating at room temperature (295 K) ', *Electrochem. Commun.*, **13** (2011) 770-773.
149. P.K. Leung, C. Ponce de León, F.C. Walsh, 'The influence of operational parameters on the performance of an undivided zinc-cerium flow battery', *Electrochim. Acta*, **80** (2012) 7-14.
150. Z.P. Xie, F.J. Xiong, D. Zhou, 'Study of the Ce^{3+}/Ce^{4+} Redox Couple in Mixed-Acid Media (CH_3SO_3H and H_2SO_4) for Redox Flow Battery Application', *Energy Fuels*, **25** (2011) 2399-2404.
151. G. Nikiforidis, W.A. Daoud, 'Effect of Mixed Acid Media on the Positive Side of the Hybrid Zinc-Cerium Redox Flow Battery', *Electrochim. Acta*, **141** (2014) 255-262.
152. G. Nikiforidis, L. Berlouis, D. Hall, D. Hodgson, 'Charge/discharge cycles on Pt and Pt-Ir based electrodes for the positive side of the Zinc-Cerium hybrid redox flow battery', *Electrochim. Acta*, **125** (2014) 176-182.
153. Z. Xie, B. Yang, D. Cai, L. Yang, 'Hierarchical porous carbon toward effective cathode in advanced zinc-cerium redox flow battery', *J. Rare Earths*, **32** (2014) 973-978.
154. Z. Xie, B. Yang, L. Yang, X. Xu, D. Cai, J. Chen, Y. Chen, Y. He, Y. Li, X. Zhou, 'Addition of graphene oxide into graphite toward effective positive electrode for advanced zinc-cerium redox flow battery', *J Solid State Electrochem.*, **19** (2015) 3339-3345.
155. Z. Na, X. Wang, D. Yin, L. Wang, 'Tin dioxide as a high-performance catalyst towards Ce(VI)/Ce(III) redox reactions for redox flow battery applications', *J. Mater. Chem. A*, **5** (2017) 5036-5043.
156. G. Nikiforidis, W.A. Daoud, 'Indium modified graphite electrodes on highly zinc containing methanesulfonate electrolyte for zinc-cerium redox flow battery', *Electrochim. Acta*, **168** (2015) 394-402.
157. G. Nikiforidis, L. Berlouis, D. Hall, D. Hodgson, 'Evaluation of carbon composite materials for the negative electrode in the zinc-cerium redox flow cell', *J. Power Sources*, **206** (2012) 497-503.
158. G. Nikiforidis, L. Berlouis, D. Hall, D. Hodgson, 'Impact of electrolyte composition on the performance of the zinc-cerium redox flow battery system', *J. Power Sources*, **243** (2013) 693-698.
159. G. Nikiforidis, L. Berlouis, D. Hall, D. Hodgson, 'A study of different carbon composite materials for the negative half-cell reaction of the zinc cerium hybrid redox flow cell', *Electrochim. Acta*, **113** (2013) 412-423.
160. G. Nikiforidis, R. Cartwright, L. Berlouis, D. Hall, D. Hodgson, 'Factors affecting the performance of the Zn-Ce redox flow battery', *Electrochim. Acta*, **140** (2014) 139-144.
161. Z. Xie, Q. Liu, Z. Chang, X. Zhang, 'The developments and challenges of cerium half-cell in zinc-cerium redox flow battery for energy storage', *Electrochim. Acta*, **90** (2013) 695-704.
162. F. Xiong, D. Zhou, Z. Xie, Y. Chen, 'A study of the Ce_3^+/Ce_4^+ redox couple in sulfamic acid for redox battery application', *Applied Energy*, **99** (2012) 291-296.
163. D.R. Martin, 'Lecture demonstrations of electrochemical reactions', J. Chem. Educ., **25** (1948) 495-497
164. J.L. Jones, A.B. Arranaga, 'A New Zinc-Iodate Primary Battery', *J. Electrochem. Soc.*, **105** (1958) 435-439.
165. B. Li, Z. Nie, M. Vijayakumar, G. Li, J. Liu, V. Sprenkle, W. Wang, 'Ambipolar zinc-polyiodide electrolyte for a high-energy density aqueous redox flow battery', *Nature Commun. 6*, (2015) Article number: 6303 https://www.nature.com/articles/ncomms7303.

166. G.M. Weng, Z. Li, G. Cong, Y. Zhou, Y.C. Lu, 'Unlocking the capacity of iodide for high-energy-density zinc/polyiodide and lithium/polyiodide redox flow batteries', *Energy & Environ. Sci.*, **3** (2017) 735-741.
167. B. Li, J. Liu, Z. Nie, W. Wang, D. Reed, J. Liu, P. McGrail, V. Sprenkle, 'Metal-Organic Frameworks as Highly Active Electrocatalysts for High-Energy Density, Aqueous Zinc-Polyiodide Redox Flow Batteries', *Nano letters*, **16** (2016) 4335-4340.
168. T. Janoschka, N. Martin, U. Martin, C. Friebe, S. Morgenstern, H. Hiller, M.D. Hager, U.S. Schubert, 'An aqueous, polymer-based redox-flow battery using non-corrosive, safe, and low-cost materials', *Nature*, **527** (2015) 78-81.
169. T. Janoschka, M.D. Hager, U.S. Schubert, 'Powering up the future: radical polymers for battery applications', *Adv. Mater.*, **24** (2012) 6397-6409.
170. S.I. Imabayashi, N. Kitamura, S. Tazuke, K. Tokuda, 'Substituent effects on electrochemical reduction of viologen dimer and trimer with ethylene spacer', *J. Electroanal. Chem.*, **239** (1988) 397-403.
171. S.I. Imabayashi, N. Kitamura, S. Tazuke, K. Tokuda, 'The role of intramolecular association in the electrochemical reduction of viologen dimers and trimers', *J. Electroanal. Chem.*, **243** (1988) 143-160.
172. J. Winsberg, T. Janoschka, S. Morgenstern, T. Hagemann, S. Muench, G. Hauffman, J. Gohy, M.D. Hager, U.S. Schubert, 'Poly(TEMPO)/Zinc Hybrid-Flow Battery: A Novel, “Green,” High Voltage, and Safe Energy Storage System', *Adv. Mater.*, **28** (2016) 2238-2243.
173. J. Winsberg, S. Muench, T. Hagemann, S. Morgenstern, T. Janoschka, M. Billing, F.H. Schacher, G. Hauffman, J.F. Gohy, S. Hoeppener, M.D. Hager, U.S. Schubert, 'Polymer/ zinc hybrid-flow battery using block copolymer micelles featuring a TEMPO corona as catholyte', *Polym. Chem.*, **7** (2016) 1711-1718.
174. Y. Xu, Y.H. Wen, J. Cheng, G.P. Cao, Y.S. Yang, 'A study of tiron in aqueous solutions for redox flow battery application', *Electrochim. Acta*, **55** (2010) 715-720.
175. A. Orita, M.G. Verde, M. Sakai, Y.S. Meng, 'The impact of pH on side reactions for aqueous redox flow batteries based on nitroxyl radical compounds', *J. Power Sources*, **321** (2016) 126-134.
176. G.W. Heise, 'Air-depolarized primary battery', US Patent 1899615 (1933).
177. S. Smedley, X.G. Zhang, 'Zinc-Air: Hydraulic Recharge, Encyclopedia of Electrochemical Power Sources', Elsevier, (2009) 393-403
178. S.I. Smedley, X.G. Zhang, 'A regenerative zinc-air fuel cell', *J. Power Sources*, **165** (2007) 897-904.
179. G. Savaskan, T. Huh, J.W. Evans, 'Further studies of a zinc-air cell employing a packed bed anode part I: discharge', *J. Appl. Electrochem.* , **22** (1992) 909-915.
180. E.A. Schumacher, 'Zinc-oxygen cells with alkaline electrolyte, Primary Battery', John Wiley & Sons Inc., **1** (1994) 265
181. Y. Li, H. Dai, 'Recent advances in zinc-air batteries', *Chem. Soc. Rev.*, **43** (2014) 5257-5275.
182. R.P. Hamlen, T.B. Atwater, 'Handbook of Batteries, Chapter 38', (2002) 1210-1262
183. P.N. Ross, 'Feasibility study of a new zinc-air battery concept using flowing alkaline electrolyte', IECEC '86; Proceedings of the Twenty-first Intersociety Energy Conversion Engineering Conference, San Diego, CA,, American Chemical Society, **2** (1986) 1066-1072
184. P.N. Ross 'Zinc-Air Design Concept for the DOE-EHP IDSEP Van'; Report no. 24639; Lawrence Berkeley Laboratory: (1988)
185. S. Muller, F. Holzer, O. Haas, 'Progress Towards 20Ah/12V Electrically Rechargeable Zinc/Air Battery', 192nd meeting of the Electrochemical Society, Paries, France, Electrochem. Soc. Proceedings, **97** (1977) 859-868
186. J. Pan, L. Ji, Y. Sun, P. Wan, J. Cheng, Y. Yang, M. Fan, 'Preliminary study of alkaline single flowing Zn-O_2 battery', *Electrochem. Comm.*, **11** (2009) 2191-2194.
187. Y.H. Wen, J. Cheng, S.Q. Ning, Y.S. Yang, 'Preliminary study on zinc-air battery using zinc regeneration electrolysis with propanol oxidation as a counter electrode reaction', *J. Power Sources*, **188** (2009) 301-307.
188. Y.H. Wen, J. Cheng, L. Zhang, X. Yan, Y.S. Yang, 'The inhibition of the spongy electrocrystallization of zinc from doped flowing alkaline zincate solutions', *J. Power Sources*, **193** (2009) 809-894.
189. C.S. BEADLEY, 'Secondary battery', US Pat. 312802, (1885).
190. P.C. Butler, D.W. Miller, A.E. Verardo, 'Flowing-electrolyte-battery testing and evolution', *17th Intersoc. Energy Conversion Eng. Conf., Los Angeles*, (1982).
191. G.P. Rajarthnam. 'The zinc/bromine flow battery: Fundamentals and novel materials for technology advancement', University of Sydney, Faculty of Engineering & Information Technologies, School of Chemical & Biomolecular Engineering, 2016.
192. Q. Lai, H. Zhang, X. Li, L. Zhang, Y. Cheng, 'A novel single flow zinc-bromine battery with improved energy density', *J. power sources*, **235** (2013) 1-4.

193. J.D. Jeon, H.S. Yang, J. Shim, H.S. Kim, J.H. Yang, 'Dual function of quaternary ammonium in Zn/Br redox flow battery: Capturing the bromine and lowering the charge transfer resistance', *Electrochim. Acta*, **127** (2014) 397-402.
194. K.J. Cathro, D. National Energy Research, D. Program, A.D.o. Resources, Energy, 'Zinc-Bromine Batteries for Energy Storage Applications', Department of Resources and Energy, (1986) https://books.google.com.hk/books?id=e0HRAAAACAAJ.
195. K.J. Cathro, K. Cedzynska, D.C. Constable, P.M. Hoobin, 'Selection of quaternary ammonium bromides for use in zinc/bromine cells', *J. Power Sources* **18** (1986) 349-370.
196. H.S. Lim, A.M. Lackner, R.C. Knechtli, 'Zinc-Bromine Secondary Battery', *J. Electrochem. Soc.*, **124** (1977) 1154-1157.
197. M. Wu, T. Zhao, H. Jiang, Y. Zeng, Y. Ren, 'High-performance zinc bromine flow battery via improved design of electrolyte and electrode', *J. Power Sources*, **355** (2017) 62-68.
198. G.P. Rajarathnam, M. Schneider, X. Sun, A.M. Vassallo, 'The Influence of Supporting Electrolytes on Zinc Half-Cell Performance in Zinc/Bromine Flow Batteries', *J. Electrochem. Soc.*, **163** (2016) A5112-A5117.
199. R. Zito, 'Zinc-bromine battery with long term stability', US Pat. 4482614, (1984).
200. P.C. Butler, P.A. Eidler, P.G. Grimes, S.E. Klassen, R.C. Miles, 'Handbook of Batteries, by D. Linden and T. B. Reddy, Chapter 39 - Zinc/Bromine Batteries', 3rd Ed. McGraw-Hill, (2002) 1-20
201. G.P. Rajarathnam, M.E. Easton, M. Schneider, A.F. Masters, T. Maschmeyer, A.M. Vassallo, 'The influence of ionic liquid additives on zinc half-cell electrochemical performance in zinc/bromine flow batteries', *RSC Advances*, **6** (2016) 27788-27797.
202. J.H. Yang, H.S. Yang, H.W. Ra, J. Shim, J.D. Jeon, 'Effect of a surface active agent on performance of zinc/bromine redox flow batteries: Improvement in current efficiency and system stability', *J. Power Sources*, **275** (2015) 294-297.
203. D. Kim, J. Jeon, 'A $Zn(ClO_4)_2$ Supporting Material for Highly Reversible Zinc-Bromine Electrolytes', *Bulletin of the Korean Chem. Soc.*, **37** (2016) 299-304.
204. M.E. Easton, P. Turner, A.F. Masters, T. Maschmeyer, 'Zinc bromide in aqueous solutions of ionic liquid bromide salts: the interplay between complexation and electrochemistry', *RSC Advances*, **5** (2015) 83674-83681.
205. Y. Munaiah, S. Dheenadayalan, P. Ragupathy, V.K. Pillai, 'High Performance Carbon Nanotube Based Electrodes for Zinc Bromine Redox Flow Batteries', *ECS J. Solid State Sci. Technol.*, **2** (2013) M3182-M3186.
206. M. Mastragostino, C. Gramellini, 'Kinetic study of the electrochemical processes of the bromine/bromine aqueous system on vitreous carbon electrodes', *Electrochim. Acta*, **30** (1985) 373-380.
207. Y. Munaiah, S. Suresh, S. Dheenadayalan, V.K. Pillai, P. Ragupathy, 'Comparative Electrocatalytic performance of single-walled and multiwalled carbon nanotubes for zinc bromine redox flow batteries', *J. Phys. Chem. C*, **118** (2014) 14795-14804.
208. L. Zhang, H. Zhang, Q. Lai, X. Li, Y. Cheng, 'Development of carbon coated membrane for zinc/bromine flow battery with high power density', *J. Power Sources*, **227** (2013) 41-47.
209. C. Wang, X. Li, X. Xi, P. Xu, Q. Lai, H. Zhang, 'Relationship between activity and structure of carbon materials for Br2/Br− in zinc bromine flow batteries', *RSC Adv.*, **6** (2016) 40169-40174.
210. C. Wang, X. Li, X. Xi, W. Zhou, Q. Lai, H. Zhang, 'Bimodal highly ordered mesostructure carbon with high activity for Br 2/Br- redox couple in bromine based batteries', *Nano Energy*, **21** (2016) 217-227.
211. D. Desai, X. Wei, D.A. Steingart, S. Banerjee, 'Electrodeposition of preferentially oriented zinc for flow-assisted alkaline batteries', *J. Power Sources*, **256** (2014) 145-152.
212. Y. Munaiah, P. Ragupathy, V.K. Pillai, 'Single-Step Synthesis of Halogenated Graphene through Electrochemical Exfoliation and Its Utilization as Electrodes for Zinc Bromine Redox Flow Battery', *J. Electrochem. Soc.*, **163** (2016) A2899-A2910.
213. H.S. Yang, J.H. Park, H.W. Ra, C.S. Jin, J.H. Yang, 'Critical rate of electrolyte circulation for preventing zinc dendrite formation in a zinc-bromine redox flow battery', *J. Power Sources*, **325** (2016) 446-452.
214. Z.G. Yang, J.L. Zhang, M.C.W. Kintner-Meyer, X.C. Lu, D.W. Choi, J.P. Lemmon, J. Liu, 'Electrochemical Energy Storage for Green Grid', *Chem. Rev., ACS*, **111** (2011) 3577-3613.
215. D.L. Douglas, J.R. Birk, 'Secondary Battery For Electrical Energy Storage', *Ann. Rev. Energy*, **5** (1980) 61-88.
216. T.R. Crompton, 'Battery Reference Book, Chapter 14', 3 Ed. Elsevier Science & Technology Books, Boston : Newnes, Oxford, England, (2000)
217. J. Jorné, J.T. Kim, D. Kralik, 'The zinc-chlorine battery: half-cell overpotential measurements', *J. Appl. Electrochem.*, **9** (1979) 573-579.

218. R.L. Doyle, M.E.G. Lyons, 'Photoelectrochemical Solar Fuel Production: From Basic Principles to Advanced Devices. Chapter 2 The Oxygen Evolution Reaction: Mechanistic Concepts and Catalyst Design ', Springer, (2016)
219. G.P. Rajarathnam, A.M. Vassallo, 'The Zn-Br Flow Battery-Materials Challenges and Practical Solutions for Technology Advancement', Springer, (2015)
220. C. Cachet, R. Wiart, 'Zinc Deposition and Passivated Hydrogen Evolution in Highly Acidic Sulphate Electrolytes: Depassivation by Nickel Impurities', *J. Appl. Electrochem.*, **20** (1990) 1009-1014.
221. H.S. Lim, A.M. Lackner, R.C. Knechtli, 'Zinc-Bromine Secondary Battery', *J. Electrochem. Soc.*, **124** (1977) 1154-1157.
222. M. Paunovic, M. Schlesinger, 'Fundamentals of Electrochemical Deposition', See R. Winand chapter 'Electrodeposition of Zinc and Zinc Alloys', 5th Ed. John Wiley & Sons, (2010) 285
223. Jr. Diaddario, L. Leonard, 'Method for Improving the Macro Throwing Power for Chloride Zinc Electroplating Baths', US Pat. 6143160, (2000).
224. A.E. Martell, 'NIST Critically Selected Stability Constants of Metal Complexes: Version 8.0', National Institute of Science and Technology (US),
225. R.K. Cannan, A. Kibrick, 'Complex formation between carboxylic acids and divalent metal cations. Journal of the American Chemical Society', *J. American Chemical Society*, **60** (1938) 2314-2320.
226. L. Li, S. Kim, W. Wang, M. Vijayakumar, Z. Nie, B. Chen, J. Zhang, G. Xia, J. Hu, G. Graff, J. Liu, Z. Yang, 'A Stable Vanadium Redox-Flow Battery with High Energy Density for Large-Scale Energy Storage', *Adv. Energy Mater.*, **1** (2011) 394-400.
227. S. Kim, M. Vijayakumar, W. Wang, J. Zhang, B. Chen, Z. Nie, F. Chen, J. Hu, Z. Yang, 'Chloride supporting electrolytes for all-vanadium redox flow batteries', *Phys. Chem. Chem. Phys.*, **13** (2011) 18186-18193.
228. C. Tang, D. Zhou, 'Methanesulfonic acid solution as supporting electrolyte for zinc-vanadium redox battery', *Electrochim. Acta*, **65** (2012) 179-184.
229. P. Leung, M.R. Mohamed, A.A. Shah, Q. Xu, M.B. Conde-Duran, 'A mixed acid based vanadium-cerium redox flow battery with a zero-gap serpentine architecture', *J. Power Sources*, **274** (2015) 651-658.
230. S. Srinivasan, M. Pushpavanam, 'Role of additives in bright zinc deposition from cyanide free alkaline baths', *J. Appl. Electrochem.*, **36** (2006) 315-322.
231. D.S. Aaron, Q. Liu, Z. Tang, G.M. Grim, A.B. Papandrew, A. Turhan, T.A. Zawodzinski, M.M. Mench, 'Dramatic performance gains in vanadium redox flow batteries through modified cell architecture', *J. Power Sources*, **206** (2012) 450-453.
232. Q.H. Liu, G.M. Grim, A.B. Papandrew, A. Turhan, T.A. Zawodzinski, M.M. Mench, 'High performance vanadium redox flow batteries with optimized electrode configuration and membrane selection', *J. Electrochem. Soc.*, **159** (2012) A1246-A1252.
233. C.A. Loto, 'Electrodeposition of Zinc from Acid Based Solutions: A Review and Experimental Study', *Asian J. Appl. Sci.*, **5** (2012) 314-326.
234. C.D. Iacovangelo, F.G. Will, 'Parametric study of zinc deposition on porous carbon in a flowing electrolyte cell', *J. Electrochem. Soc.*, **132** (1985) 851-857.
235. K. Sato, K. Yamato, K. Iozumi, 'Manufacturing of One-side Electrogalvanized Steel Strip with Heavy Coating', *Transactions ISIJ*, **23** (1983) 946-953.
236. J.F. Silva Filho, V.F.C. Lins, 'Crystallographic texture and morphology of an electrodeposited zinc layer', *J. Surf. Coat. Technol.* , **200** (2006) 2892-2899.
237. H. Park, J.A. Szpunar, 'The role of texture and morphology in optimizing the corrosion resistance of zinc-based electrogalvanized coatings', *Corrosion Science*, **40** (1998) 525-545.
238. Y.A. Naik, T.V. Venkatesha, 'A new condensation product for zinc plating from non-cyanide alkaline bath', *Bull. Mater. Sci.*, **28** (2005) 495-501.
239. Y.A. Naik, T.V. Venkatesha, P.V. Nayak, 'Electrodeposition of Zinc from Chloride Solution ', *Turk. J. Chem.*, **26** (2002) 725-733.
240. G. Achary, H.P. Sachin, Y. Arthoba Naik, T.V. Venkatesha, 'Effect of a new condensation product on electrodeposition of zinc from a non-cyanide bath', *J. Bull. Mater. Sci.*, **30** (2007) 219-224.
241. Y. Arthoba NAIK, T.V. Venkatesha, P. Vasudeva, 'Electrodeposition of zinc from chloride solution', *Turk J. Chem.*, **26** (2002) 725 -733.
242. T.J. Tuaweri, E.M. Adigio, P.P. Jombo, 'A Study of Process Parameters for Zinc Electrodeposition from a Sulphate Bath', *Int. J. Engin. Sci. Invention*, **2** (2013) 17-24.
243. S. Afifi, A. Ebaid, M. Hegazy, K. Donya, 'On the electrowinning of zinc from alkaline zincate solutions', *J. Electrochem. Soc.* , **138** (1991) 1929-1933.
244. A.L. Marshall, 'The electrodeposition of zinc from sulphate solutions', *Trans. Faraday Soc.*, **21** (1925) 297-314.

245. G. Nikiforidis, L. Berlouis, D. Hall, D. Hodgson, 'A study of different carbon composite materials for the negative half-cell reaction of the zinc cerium hybrid redox flow cell', *Electrochim. Acta*, **113** (2013) 412- 423.
246. F. Galvani, I.A. Carlos, 'The effect of the additive glycerol on zinc electrodeposition on steel', *J. Met. Finish.*, **95** (1997) 70-72.
247. S. Martin, 'Zinc Electroplating and Baths therefore Containing Carrier Brighteners', US Pat. 4541906, (1985).
248. D.R. Gabe, 'The role of hydrogen in metal electrodeposition processes', *J. Appl. Electrochem.*, **27** (1997) 908-915.
249. L. Mirkova, G. Maurin, I. Krastev, C. Tsvetkova, 'Hydrogen evolution and permeation into steel during zinc electroplating; effect of organic additives', *J. Appl. Electrochem.*, **31** (2001) 647-654.
250. M.H. Abd Elhamid, B.G. Ateya, K.G. Weil, H.W. Pickering, 'Calculation of the hydrogen surface coverage and rate constants of the hydrogen evolution reaction from polarization', *J. Electrochem. Soc.*, **147** (2000) 2148-2150.
251. T. Zakroczymski, V. Kleshnya, J. Flis, 'Evolution and Entry of Hydrogen into Iron during Cathodic Charging in Alkaline Solution with Ethylenediaminetetraacetic Acid', *J. Electrochem. Soc.*, **145** (1998) 1142-1148.
252. D.M. Drazic, B.E. Conway, J.O.M. Bockris, R.E. White, 'Modern Aspects of Electrochemistry', Plenum Press, New York, **19** (1989)
253. H. Vehoff, H. Wipf, 'Tropics in Applied Physics', Springer Verlag, Berlin, **73** (1997)
254. J.L. Zhu, Y.H. Zhou, C.Q. Gao, 'Influence of surfactants on electrochemical behavior of zinc electrodes in alkaline solution', *J. Power Sources*, **72** (1998) 231-235.
255. M. Maja, N. Penazzi, G. Farnia, G. Sandona, 'Zinc corrosion in NH_4Cl and effect of some organic inhibitors', *Electrochim. Acta*, **38** (1993) 1453-1459.
256. C. Cachet, M. Keddam, V. Mariotte, R. Wiart, 'Influence of Perfluorinated and Hydrogenated Surfactants upon Hydrogen Evolution on Gold Electrodes', *Electrochim. Acta*, **39** (1994) 2743-2750.
257. C. Juhel, B. Beden, C. Lamy, J.M. Leger, R. Vignaud, 'Effect of surfactant Forafac on hydrogen evolution on a zinc electrode', *Electrochim. Acta*, **35** (1990) 479-481.
258. A. Gomes, M.I. da Silva Pereira, 'Zn electrodeposition in the presence of surfactants: Part I. Voltammetric and structural studies', *Electrochim. Acta*, **52** (2006) 863-871.
259. C. Cachet, Z. Chami, R. Wiart, 'Electrode kinetics connected to deposit growth for zinc electrodeposition: Influence of surfactants', *Electrochim. Acta*, **32** (1987) 465-474.
260. C.D. Iacovangelico, F.G. Will, ' *J. Electrochem. Soc.*, **132** (1985) 851.
261. C. Cachet, R. Wiart, 'Influence of a perfluorinated surfactant on the mechanism of zinc deposition in acidic electrolytes ', *Electrochim. Acta* **44** (1999) 4743-4751.
262. C.W. Lee, K. Sathiyanarayanan, S.W. Eom, H.S. Kim, M.S. Yun, 'Novel electrochemical behavior of zinc anodes in zinc/air batteries in the presence of additives ', *J. Power Sources*, **159** (2006) 1474-1477.
263. F. Ganne, C. Cachet, G. Maurin, R. Wiart, E. Chauveau, J. Petitjean, 'Impedance spectroscopy and modelling of zinc deposition in chloride electrolyte containing a commercial additive', *J. Appl. Electrochem.*, **30** (2000) 665-673.
264. R. Ichino, C. Cachet, R. Wiart, 'Mechanism of zinc electrodeposition in acidic sulfate electrolytes containing Pb^{2+} ions', *Electrochim. Acta*, **41** (1996) 1031-1039.
265. S. Thomson, N. Birbilis, M.S. Venkatraman, I.S. Cole, 'Corrosion of Zinc as a Function of pH', *Corrosion Science Edition*, **68** (2012) 015009-1 - 015009-9.
266. A.M. Alfantazi, D.B. Dreisinger, 'The Role of Zinc and Sulfuric Acid Concentrations on Zinc Electrowinning from Industrial Sulfate Based Electrolyte', *J. Appl. Electrochem.*, **31** (2001) 641-646.
267. M.S. Youssef, C.C. Koch, P. S. Fedkiw, ' *J. Corros. Sci.*, **46** (2004) 51.
268. Kh. Saber, C.C. Koch, P.S. Fedkiw, 'Pulse current electrodeposition of nanocrystalline zinc ', *J. Mater. Sci. Eng.* , **A341** (2003) 174-181.
269. B. Kavitha, P. Santhosh, M. Renukadevi, A. Kalpana, P. Shakkthivel, T. Vasudevan, 'Role of organic additives for zinc plating', *J. Surf. Coat. Technol.*, **201** (2006) 3438-3442.
270. G.B. Adams, 'Electrically rechargeable battery', US Pat. 4180623, 25/12/1979.
271. M. Pownall, 'Back to the future with battery development'. Business News Western Australia, https://www.businessnews.com.au/article/Back-to-the-future-with-battery-development accessed on 3 Aug 2017.
272. 'EnergyPod® 2 - Long Duration Energy Storage'. Primus Power, http://primuspower.com/en/product/ accessed on 3 Aug 2017.
273. P. Alotto, M. Guarnieri, F. Moro, 'Redox flow batteries for the storage of renewable energy: A review', *Renewable and Sustainable Energy Reviews*, **29** (2014) 325-335.

274. D. Vissers, W. DeLuca, G. Henriksen, 'Advanced Batteries for Electric Vehicle Applications', Symposium proceedings of the ACS Meeting, Chicago, Illinois, (1993) https://www.osti.gov/scitech/servlets/purl/139698.
275. P.T. Moseley, J. Garche, 'Electrochemical Energy Storage for Renewable Sources and Grid Balancing, Chapter 17: Redox Flow Batteries', 1st Ed. Elsevier, (2015) 309-336,
276. D. Linden, T.B. Reddy, 'Handbook of Batteries', 3rd Ed. McGraw-Hill, (2002) 243-274